NASA Technical Memorandum 108847

Dynamic Response of NASA Rotor Test Apparatus and Sikorsky S-76 Hub Mounted in the 80- by 120-Foot Wind Tunnel

Randall L. Peterson, Ames Research Center, Moffett Field, California
Muhammed S. Hoque, Sterling Federal Systems, Inc., Palo Alto, California

September 1994

National Aeronautics and
Space Administration

Ames Research Center
Moffett Field, California 94035-1000

Dynamic Response of NASA Rotor Test Apparatus and Sikorsky S-76 Hub Mounted in the 80- by 120-Foot Wind Tunnel

RANDALL L. PETERSON AND MUHAMMED S. HOQUE*

Ames Research Center

Abstract

A shake test was conducted in the 80- by 120-Foot Wind Tunnel at NASA Ames Research Center, using the NASA Ames Rotor Test Apparatus (RTA) and the Sikorsky S-76 rotor hub. The primary objective of this shake test was to determine the modal properties of the RTA, the S-76 rotor hub, and the model support system installed in the wind tunnel. Random excitation was applied at the rotor hub, and vibration responses were measured using accelerometers mounted at various critical locations on the model and the model support system. Transfer functions were computed using the load cell data and the accelerometer responses. The transfer function data were used to compute the system modal parameters with the aid of modal analysis software.

Introduction

A shake test in the 80- by 120-Foot Wind Tunnel was conducted to determine the modal parameters (natural frequency, modal mass, and damping) of RTA/S-76 rotor hub consisting of tunnel balance, turntable, struts, and model, as shown in figures 1 and 2. The primary objective of the shake test was to determine the support system modal frequencies and damping values to be used in a comprehensive rotor analysis code to predict the potential ground resonance stability boundaries (ref. 1, ch. 12).

Ground resonance is a mechanical phenomenon that occurs when the rotor, operated within a certain rotor speed range, experiences coupling between a rotor in-plane mode and a model support system mode, thus causing excessive vibration in the mechanical system. In the absence of sufficient damping in the rotor in-plane mode or the model support system, excessive vibration can result in significant damage to the model and, consequently, the wind tunnel facility. Therefore, the modal parameters obtained from the shake test are used in a rotorcraft dynamics analysis to predict the minimum amount of damping necessary from participating modes for safe operation of the rotor in the critical rotor speed range in the wind tunnel facility.

*Sterling Federal Systems, Inc., Palo Alto, California.

The RTA/S-76 hub configuration was excited using random excitation applied at the hub/shaft adapter interface, as shown in figures 2–4. The total blade mass was simulated by an additional fixture that spanned the instrumentation hat of the S-76 rotor hub. The hub accelerometers were mounted along the three orthogonal axes on the simulated hub shake fixture. The hub response function is defined as the ratio of accelerometer response at the hub, along a given direction, to the force applied near the hub along the same direction. The shake tests were performed along parallel and perpendicular directions at 0-deg and 90-deg model yaw with respect to the wind tunnel flow direction, as shown in figures 3 and 4. In this study, longitudinal and lateral directions are defined with respect to the RTA body and model support system.

The model was also shaken at 90-deg yaw to determine the dynamic characteristics of this setup for rotor hover testing in the 80- by 120-Foot Wind Tunnel test section.

Test System Description

Model

The RTA model with all the hardware installed weighed approximately 34,400 lb. This weight consists of two 1,500-hp motors, gearbox, rotor balance, RTA frame, Sikorsky S-76 hub, and the RTA fairing. The model was mounted on a combination of 12-ft 80- by 120-Foot Wind Tunnel main struts, 15-ft 40- by 80-Foot Wind Tunnel main struts, and 60-in. strut tips. The distance between the strut attachment point on the model and the hub was approximately 10 ft, which located the hub approximately 43 ft above the tunnel floor.

Test Apparatus

An 1,100-lb capacity hydraulic actuator was used to excite the model and the support system at the hub/shaft adapter interface, which was about 16 in. below the hub centerline. One end of the hydraulic actuator was attached to a 5-ft-long extension arm, and the other end was attached to the hub/shaft adapter interface (fig. 2). The

extension arm was attached to a large reaction mass (11,600 lb) suspended from a gantry crane, as shown in figures 1 and 2. The shaker was aligned with respect to the extension arm, which was, in turn, aligned parallel to each of the shake directions (longitudinal or lateral, 0-deg or 90-deg model yaw; figs. 3 and 4), to minimize excitation of modes in directions orthogonal to the shake direction. After initially achieving rough alignment with the extension arm using the gantry crane, the actuator was better aligned by applying tension to the guy wires attached between the reaction mass and tunnel floor. The guy wires also served the purpose of restraining the reaction mass from swaying during excitation.

A load cell placed between the hydraulic actuator and the hub/shaft adapter clevis measured the applied force. Accelerometers were mounted on the hub/rotor-blade mass simulation hardware, the RTA frame and transmission, the struts, and the balance T-frame (fig. 2). These accelerometer mounting locations were selected to provide large acceleration response to better understand the vibratory modes of the model, struts, and balance frame. The following is a description of the locations of accelerometers.

1. Lateral and longitudinal hub accelerometers were mounted on the hub/rotor blade mass simulation hardware.

2. Longitudinal and lateral accelerometers were mounted at the metric side of the rotor balance.

3. Lateral, longitudinal, and vertical accelerometers were mounted at the front section of the RTA frame along the centerline of the body axis.

4. Lateral and longitudinal accelerometers were mounted at the tail end of the RTA frame along the centerline of the body axis.

5. One vertical accelerometer was mounted on the gearbox.

6. Lateral and longitudinal accelerometers were mounted on both sides of the model next to the strut attachment points.

7. Lateral and longitudinal accelerometers were mounted on the left strut at the interface between the 40- by 80- and the 80- by 120-Foot Wind Tunnel struts, which could also be relocated to the interface on the right strut for further analysis of the strut mode shape.

8. Lateral and longitudinal accelerometers were mounted on the balance T-frame (fig. 2).

9. Two vertical accelerometers located diametrically opposite each other and in line with the direction of excitation were mounted on the hub/rotor-blade mass simulation hardware. These transducers were installed to measure the rolling and pitching moment input by the actuator onto the rotor hub.

Although 20 accelerometers were used along with a load cell providing 21 output signals, transfer function data from only 16 channels could be acquired during a particular shake. Transfer function data were acquired and stored using a 16-channel GenRad 2515 Computer-Aided Testing System. This system is a portable digital signal processor for general purpose data acquisition and analysis. Data in the frequency range from DC to 25.6-kHz AC signal, with alias protection on all channels, can be acquired and analyzed by this system.

Test Procedures

As an initial study of the system response, the GenRad acquisition mode was set to acquire data in a frequency range from 0 to 128 Hz to capture the overall response of the dynamic system, which consists of the RTA shaft, upper housing, rotor balance, the transmission, and the RTA frame. Data were also acquired in the frequency range of 0 to 32 Hz to increase the resolution of the transfer function for low frequencies. The test matrix for the lateral and longitudinal shake test are shown in table 1. The applied random force values are 1/2 peak to peak.

Results

Data

Figures 5 and 6 correspond to a lateral shake (0-deg model yaw) without and with the balance T-frame snubbers engaged, respectively. In a frequency bandwidth of 0 to 32 Hz there were five modes associated with figure 5. The low frequency modes, the first two peaks at 1.63 and 2.31 Hz, are support system modes, and the last two, at 14.06 and 24.19 Hz, are attributed to RTA upper housing/rotor-shaft and frame modes.

In figure 6, the peak at 1.63 Hz, associated with the balance T-frame, disappears due to engagement of the balance snubbers. The strut mode (2.31 Hz; fig. 5) drops to 2.0 Hz due to the engagement of the balance snubbers. This shift in frequency is most likely due to the combined effects of change in the modal stiffness and modal mass associated with this vibratory mode as a result of elimination of the balance T-frame mode. There is another noticeable difference between figures 5 and 6 around the 14.06-Hz mode. As seen in figure 6, a mode at 13.44 Hz begins forming, possibly because more vibratory energy is available to excite these RTA upper housing modes

with the balance snubbers engaged. Mode 4, at 24.19 Hz, is also attributed to RTA frame modes.

Figures 7 and 8 correspond to a lateral shake (90-deg model yaw) without and with the balance T-frame snubbers engaged, respectively. In figure 7, four modes at 1.38, 2.19, 13.94, and 24.75 Hz appear in a bandwidth of 0 to 32 Hz. These modes were identified as balance T-frame, strut, RTA upper housing/rotor-shaft, and RTA frame modes. When the snubbers are engaged, the balance T-frame mode is eliminated (mode 2; fig. 8), but other modes began forming in the frequency ranges of 12 to 15 Hz and 22 to 26 Hz, which were attributed to the RTA frame.

Figures 9 and 10 correspond to a longitudinal shake (0-deg model yaw) without and with the balance T-frame snubbers engaged, respectively. The flexibility of the RTA frame and other mechanical components on the RTA is better illustrated in this shake configuration. There are at least 12 distinct modes, of which 1.25- and 1.94-Hz modes (fig. 9) have been attributed to the support system. The remaining modes are associated with the RTA frame. When the balance snubbers are engaged the balance mode is suppressed, and all the other modes maintain the same frequency as the snubbers disengaged configuration except modes 2 and 3 (fig. 9). These two modes may have shifted due to the change in the system stiffness due to the change in configuration resulting from balance snubber engagement. There is another noticeable difference between figures 9 and 10; that is, the relative magnitude of modes 3–5 drops with the engagement of the balance snubbers, which cannot be explained at this stage without further experimentation.

Figures 11 and 12 correspond to a longitudinal shake (90-deg model yaw) without and with the balance T-frame snubbers engaged, respectively. In the balance snubbers disengaged configuration (fig. 11), the mode at 1.56 Hz has a higher response amplitude than the peak at 2.25 Hz, whereas in the snubbers engaged configuration (fig. 12) the latter mode (2.25 Hz) has been eliminated, thus allowing the first mode, which has shifted from 1.56 to 1.75 Hz, to respond with a higher amplitude. From this behavior of mode suppression and mode shift, it cannot be concluded with certainty that mode 1 (1.56 Hz) is due to the strut vibration and mode 2 (2.25 Hz) is due to the balance T-frame without extensive mode shape analysis. The peaks above 6.0 Hz are associated with the RTA frame and are not relevant to a ground resonance stability analysis.

Analysis Techniques

The data were analyzed using the Structural Dynamics Research Corporation Modal Plus software package (ref. 2). Modal Plus provides four methods to determine the modal parameters from frequency response functions. These four methods are Search Peak, Complex Exponential, Direct Parameter, and Polyreference Method.

The *Search Peak* method computes a good estimate of the modal parameters and fits a smooth curve over the transfer function using these estimated modal parameters, provided the resonant peaks are well defined (i.e., at least a couple of hertz apart and can be modeled as second-order single degree of freedom systems).

For resonant peaks that are close to each other, the *Complex Exponential* technique, a time domain algorithm, computes a better estimate of modal parameters at the resonant peaks of the transfer function.

The *Direct Parameter* method is a frequency domain, multiple degree of freedom curve fitting algorithm that computes a global estimate of the modal characteristics from several response locations with respect to a single excitation/reference location.

The *Polyreference Method* is a time domain complex exponential algorithm capable of multiple degree of freedom curve fitting providing a global estimate of modal parameters with respect to two or more excitation/reference locations.

Since the resonant peaks in most of these transfer functions are only a few hertz apart, the Complex Exponential technique provided better curve-fits of the data than the Search Peak method for the frequency range of interest (i.e., 1.0–3.0 Hz). This technique computes polynomial coefficients in each of the time subintervals and steps through all the subintervals of the total time record, until the entire time history is curve-fitted, using the specified resonant frequencies and the computed polynomial coefficients. These coefficients are then used to compute the residues corresponding to each of the specified resonant peaks on the original curve, from which the modal parameters are then computed (ref. 2, ch. 6).

In actual usage of the analysis software only, the frequency range of interest and the number of resonant peaks on the original transfer function need be specified to obtain a curve-fit. For the purposes of ground resonance stability testing, frequencies of up to 1/rev would be chosen. During modal parameter estimation at the resonant peaks, the analysis method assigns a default number of roots that is greater than the specified number of resonant peaks. From experience it has been

determined that allowing the algorithm to compute the default number of roots (nonphysical mathematical and actual roots) leads to better estimates of natural frequencies and, consequently, better modal parameters. These mathematical roots are distinguishable from the real roots on the complete list of roots either because the magnitudes of the residues are very small or the phase is close to 0 or π radians. Once all the roots have been computed the mathematical roots can be suppressed, beginning with the most obvious mathematical roots. The final curve-fit is obtained by adding residual corrections to the curve-fit, away from the resonant peaks, to better fit the original transfer function.

Discussion of Results

Figure 13 is a curve-fit of the first two modes of figure 5 for the lateral 0-deg model yaw shake without the balance T-frame snubbers engaged. A curve-fit of the first two modes in this narrow frequency range (1.0–3.0 Hz) was compared with a broader band curve-fit, from which it was determined that the narrow-band curve-fit yielded a better curve-fit than the broader band. From previous experience (ref. 3) it can be concluded that the modal parameters derived from narrow-band curve-fit are more accurate because the influence of the other modes is excluded; therefore, modal parameters were computed using the narrow-band curve-fit parameters. The first mode has been attributed to the RTA/balance T-frame yaw/rotational mode even though the modal mass is less than the expected balance T-frame mode executing translation motion (table 2).

These strut modal masses are somewhat smaller than expected because the RTA model itself weighs 34,400 lb. In the strut mode of vibration the RTA mass can be assumed to act as a concentrated mass at the end of a cantilever beam with spring (balance snubbers disengaged) or fixed (snubbers engaged) restraints. Therefore, the modal mass of the strut mode should be the sum of the mass of the RTA and some fraction of the mass of the struts. Since the computed modal masses are smaller than the RTA mass itself, it can only be concluded that these modes are not purely translational modes, but rather a combination of the translational and rotational modes.

Figure 14 is a curve-fit of the first mode of the transfer function shown in figure 6 with the balance T-frame snubbers engaged. The curve-fit result shown in figure 6 is a narrower peak than that of the original curve, implying that the value of critical damping ratio for this peak would be lower than if the curve-fit had been an exact one, thus providing a conservative estimate.

The curve-fits of transfer functions (figs. 7 and 8), obtained from the lateral 90-deg model yaw shake without and with balance T-frame snubbers engaged, are shown in figures 15 and 16. The balance T-frame and strut modes are at 1.41 Hz and 2.16 Hz, respectively. The first mode has been attributed to the balance T-frame mode because of transfer function amplitude and broadness of the peak compared to the second peak that has been attributed to the strut mode. These attributes of the support system modes are confirmed by the modal masses computed from the curve-fit parameter (table 2), which are 3,604 and 1,025 slugs for the balance T-frame and strut modes, respectively.

The longitudinal 0-deg model yaw shake transfer function, without and with the balance T-frame snubbers engaged, are presented in figures 9 and 10, respectively, and their corresponding curve-fits are shown in figures 17 and 18, respectively. The curve-fit in figure 17 is a very good representation of the original transfer function in this frequency range (0.5–3.0 Hz). The modal masses of the support system modes obtained from this curve-fit are representative of the balance T-frame and combined RTA/strut modes. Likewise, the modal mass of the RTA/strut mode, with the balance T-frame snubbers engaged shake configuration, is representative of the assumed translational modal mass.

Curve-fits of the transfer functions (figs. 11 and 12) obtained from the longitudinal 90-deg model yaw shake configurations, without and with the balance T-frame snubber engaged, are shown in figures 19 and 20. The modal masses and the amplitudes of the transfer function of the first two modes in figures 11 and 19 indicate that the second mode is the balance T-frame and the first mode is the strut mode. However, this conclusion cannot be reached without more detailed mode shape evaluation.

Tabulated Modal Parameters

Tables 2 and 3 are composite listings of the modal parameters, in physical units, corresponding to the physical modes of vibration of the model support system structure. From the reduced data it has been determined that there is at least 1.9 percent critical damping in all modes of vibration for configurations with the balance snubbers engaged and 2.6 percent critical damping for configurations with the balance snubbers disengaged.

Mode Shapes

A stick model (fig. 21) of the transducer setup illustrates the strategic location of these transducers. The coordinate geometry is listed in table 4, where the origin is located at node 7. The structural responses of nodes 2–5 were set

equal to the response at node 1, because it was assumed that there is no structural flexibility between node 1 and the above mentioned nodes. Nodes 9 and 10, as shown in figure 21, were supposed to define the center of gravity and the intersection between nodes 11 and 12, respectively. In the stick model they were defined as coincident since there were no response measurements available at either of these two locations. A linear interpolation of the mode shapes between nodes 11 and 12 provided the response at nodes 9 and 10. The mode shape coefficient at node 7 was obtained from a linear interpolation between nodes 8 and 10, and the response at node 6 was obtained from a linear interpolation of responses between nodes 1 and 7. Interpolation of the mode shapes at nodes 11 and 12 also provided the nodal response at node 13. The response at node 14 was derived from the responses of nodes at 11, 12, and 15. The responses at nodes 16 and 17 were derived from transducer responses at either node 18 or 20 combined with the values of nodes at 11–13.

Figures 22 and 23 depict the mode shapes of the first two modes of vibration for the lateral shake configuration, without the balance T-frame snubbers engaged and the model at 0-deg yaw. The corresponding mode shape coefficients at each of the mode shapes are listed in tables 5 and 6 for figures 22 and 23, respectively. Likewise, figure 24 illustrates the maximum deflection of the structure at the only vibration mode, normalized with respect to the hub lateral response, for lateral shake at 0-deg model yaw and the balance scales locked. The corresponding mode shape coefficients are tabulated in table 7.

Figure 25 and 26 depict the mode shapes of the first two modes of vibration for the longitudinal shake with the model yawed at 0 deg and balance T-frame snubbers disengaged. The mode shape coefficients for figures 25 and 26 are tabulated in tables 8 and 9, respectively. Likewise, figure 27 illustrates the mode shape of the only vibration mode due to longitudinal shake at 0-deg model yaw with the balance T-frame snubbers engaged, and the mode shape coefficients are tabulated in table 10. The mode shapes for lateral and longitudinal shakes with the model yawed at 90 deg are not presented here because they look much the same as the above modes.

Conclusions

The shake test revealed all the low frequency modes of vibration of the wind tunnel model support system for the RTA and S-76 rotor mounted in the NASA Ames 80- by 120-Foot Wind Tunnel. These modal parameters will be used in a comprehensive analytical model to predict the stability of the rotor and model support system in performing a wind tunnel test in the 80- by 120-Foot Wind Tunnel facility.

References

1. Johnson, W.: Helicopter Theory. Princeton University Press, 1980.
2. User's Manual for MODAL-PLUS 9.0, Copyright 1985, General Electric CAE International.
3. Hoque, M. S.; and Graham, T. A.: Dynamic Characteristics of Bell M412 and Model 576 Test Stand in the 40- by 80-Foot Wind Tunnel. NASA TM-102880, Apr. 1991.

Table 1. Test matrix for lateral and longitudinal shake test

Force, lb, approx.	Frequency, Hz	Yaw, deg	Balance T-frame snubbers
400	0–128	0	Disengaged
400	0–64	0	Disengaged
400	0–32	0	Disengaged
200	0–64	0	Disengaged
200	0–32	0	Disengaged
100	0–32	0	Disengaged
400	0–128	0	Engaged
400	0–64	0	Engaged
400	0–32	0	Engaged
200	0–64	0	Engaged
200	0–32	0	Engaged
400	0–128	90	Disengaged
400	0–64	90	Disengaged
400	0–32	90	Disengaged
200	0– 32	90	Disengaged
400	0–64	90	Engaged
400	0–32	90	Engaged
300	0–32	90	Engaged
200	0–32	90	Engaged

Table 2. Modal properties for lateral shake test of the RTA/S-76 in the 80- by 120-Foot Wind Tunnel, 0-deg and 90-deg yaw, balance T-frame snubbers disengaged and engaged

Mode	Frequency, Hz	Viscous damping ratio, %	Modal amplitude, g-rad/(lb-s)	Phase, radians	Modal mass, slug	Modal damping, lb/ft	Modal stiffness, lb-sec/ft
Balance T-frame snubbers disengaged, 0-deg yaw							
Balance	1.678	5.815	2.38139E-04	–1.383	689	845	76,610
Strut	2.322	4.632	2.82915E-04	–1.930	802	1,084	170,766
Balance T-frame snubbers engaged, 0-deg yaw							
Strut	1.981	2.234	4.14674E-04	–1.543	467	259	72,287
Balance T-frame snubbers disengaged, 90-deg yaw							
Balance	1.407	7.130	3.82129E-05	–1.399	3604	4,544	281,698
Strut	2.155	2.697	2.05404E-04	–1.591	1025	748	187,886
Balance T-frame snubbers engaged, 90-deg yaw							
Strut	2.017	1.984	2.00142E-04	–1.447	984	495	158,077

Table 3. Modal properties for longitudinal shake test of the RTA/S-76 in the 80- by 120-Foot Wind Tunnel, 0-deg and 90-deg yaw, balance T-frame snubbers disengaged and engaged

Mode	Frequency, Hz	Viscous damping ratio, %	Modal amplitude, g-rad/(lb-s)	Phase, radians	Modal mass, slug	Modal damping, lb/ft	Modal stiffness, lb-sec/ft
Balance T-frame snubbers disengaged, 0-deg yaw							
Balance	1.289	12.199	4.50647E-05	–1.527	2,814	5,560	90,536
Strut	1.934	3.813	1.28422E-04	–1.669	1,472	1,364	47,346
Balance T-frame snubbers engaged, 0-deg yaw							
Strut	1.729	2.046	1.33025E-04	–1.532	1,269	564	40,842
Balance T-frame snubbers disengaged, 90-deg yaw							
Balance	1.577	4.297	1.03651E-04	–1.284	1,487	1,266	47,842
Strut	2.227	8.480	3.41026E-05	–1.756	6,399	15,187	205,897
Balance T-frame snubbers engaged, 90-deg yaw							
Strut	1.720	2.373	1.33245E-04	–1.556	1,261	647	40,565

Table 4. Nodal coordinates of the stick model representation of the RTA in the 80- by 120-Foot Wind Tunnel

Node	X location	Y location	Z location
1	0.0	0.0	134.0
2	0.0	12.0	134.0
3	0.0	–12.0	134.0
4	–12.0	0.0	134.0
5	12.0	0.0	134.0
6	0.0	0.0	48.0
7	0.0	0.0	0.0
8	–72.0	0.0	0.0
9	37.0	0.0	0.0
10	37.0	0.0	0.0
11	37.0	49.0	0.0
12	37.0	–49.0	0.0
13	215.0	0.0	0.0
14	37.0	49.0	–252.0
15	37.0	–49.0	–252.0
16	37.0	49.0	–396.0
17	37.0	–49.0	–396.0
18	37.0	0.0	–396.0
19	126.0	0.0	–396.0
20	215.0	0.0	–396.0

Table 5. Mode shape coefficients, mode 1, lateral shake, 0-deg yaw, snubbers disengaged

Node	X coefficient	Y coefficient	Z coefficient
1	1.580E-05	–3.283E-04	0.000E-01
2	1.580E-05	–3.283E-04	0.000E-01
3	1.580E-05	–3.283E-04	0.000E-01
4	1.580E-05	–3.283E-04	0.000E-01
5	1.580E-05	–3.283E-04	0.000E-01
6	1.012E-05	7.850E-05	0.000E-01
7	6.948E-06	3.074E-04	0.000E-01
8	5.332E-04	4.030E-04	0.000E-01
9	–1.077E-05	2.582E-04	0.000E-01
10	–1.077E-05	2.582E-04	0.000E-01
11	3.261E-05	2.678E-04	0.000E-01
12	–5.422E-05	2.486E-04	0.000E-01
13	–4.348E-05	–6.716E-05	0.000E-01
14	5.567E-05	1.895E-04	0.000E-01
15	4.003E-05	1.521E-04	0.000E-01
16	–1.352E-05	9.036E-05	0.000E-01
17	–1.352E-05	9.036E-05	0.000E-01
18	–1.352E-05	9.036E-05	0.000E-01
19	1.741E-06	3.188E-05	0.000E-01
20	1.705E-05	–2.652E-05	0.000E-01

Table 6. Mode shape coefficients, mode 2, lateral shake, 0-deg yaw, snubbers disengaged

Node	X coefficient	Y coefficient	Z coefficient
1	3.102E-05	–3.899E-04	0.000E-01
2	3.102E-05	–3.899E-04	0.000E-01
3	3.102E-05	–3.899E-04	0.000E-01
4	3.102E-05	–3.899E-04	0.000E-01
5	3.102E-05	–3.899E-04	0.000E-01
6	–8.223E-06	9.269E-05	0.000E-01
7	–1.462E-04	3.641E-04	0.000E-01
8	–4.167E-04	4.536E-04	0.000E-01
9	1.326E-05	3.180E-04	0.000E-01
10	1.326E-05	3.180E-04	0.000E-01
11	5.185E-05	3.274E-04	0.000E-01
12	–2.526E-05	3.091E-04	0.000E-01
13	1.765E-05	4.259E-05	0.000E-01
14	5.154E-05	1.427E-04	0.000E-01
15	2.370E-05	1.169E-04	0.000E-01
16	5.050E-05	1.258E-04	0.000E-01
17	4.997E-06	1.258E-04	0.000E-01
18	5.025E-06	1.258E-04	0.000E-01
19	8.306E-08	8.690E-05	0.000E-01
20	–4.776E-06	4.806E-05	0.000E-01

Table 7. Mode shape coefficients, mode 1, lateral shake, 0-deg yaw, snubbers engaged

Node	X coefficient	Y coefficient	Z coefficient
1	2.046E-04	–1.537E-03	1.131E-05
2	2.046E-04	–1.537E-03	1.131E-05
3	2.046E-04	–1.537E-03	1.131E-05
4	2.046E-04	–1.537E-03	1.131E-05
5	2.046E-04	–1.537E-03	1.131E-05
6	–2.170E-04	4.084E-04	2.982E-06
7	–1.436E-04	1.456E-03	2.982E-06
8	–8.802E-04	1.843E-03	4.163E-06
9	2.889E-04	1.230E-03	0.000E-01
10	2.889E-04	1.230E-03	0.000E-01
11	3.134E-04	1.266E-03	0.000E-01
12	–2.453E-05	1.187E-03	0.000E-01
13	9.874E-05	–1.380E-04	0.000E-01
14	3.193E-04	7.305E-04	0.000E-01
15	3.437E-04	7.305E-04	0.000E-01
16	0.000E-01	0.000E-01	0.000E-01
17	0.000E-01	0.000E-01	0.000E-01
18	0.000E-01	0.000E-01	0.000E-01
19	0.000E-01	0.000E-01	0.000E-01
20	–3.151E-06	2.149E-05	0.000E-01

Table 8. Mode shape coefficients, mode 1, longitudinal shake, 0-deg yaw, snubbers disengaged

Node	X coefficient	Y coefficient	Z coefficient
1	–3.261E-05	–1.163E-05	0.000E-01
2	–3.261E-05	–1.163E-05	0.000E-01
3	–3.261E-05	–1.163E-05	0.000E-01
4	–3.261E-05	–1.163E-05	0.000E-01
5	–3.261E-05	–1.163E-05	0.000E-01
6	–3.720E-05	5.640E-06	0.000E-01
7	–3.980E-05	1.536E-05	0.000E-01
8	–3.980E-05	1.536E-05	0.000E-01
9	–3.980E-05	1.536E-05	0.000E-01
10	–3.980E-05	1.536E-05	0.000E-01
11	–3.662E-05	1.015E-05	0.000E-01
12	–4.303E-05	1.967E-05	0.000E-01
13	–3.980E-05	1.536E-05	0.000E-01
14	–3.919E-05	1.206E-05	0.000E-01
15	–3.919E-05	1.206E-05	0.000E-01
16	–2.501E-05	2.384E-06	0.000E-01
17	–2.501E-05	2.384E-06	0.000E-01
18	–2.501E-05	2.384E-06	0.000E-01
19	–2.501E-05	2.384E-06	0.000E-01
20	–2.501E-05	2.384E-06	0.000E-01

Table 9. Mode shape coefficients, mode 2, longitudinal shake, 0-deg yaw, snubbers disengaged

Node	X coefficient	Y coefficient	Z coefficient
1	–2.724E-04	–1.671E-04	–8.154E-06
2	–2.724E-04	–1.671E-04	–8.154E-06
3	–2.724E-04	–1.671E-04	–8.154E-06
4	–2.724E-04	–1.671E-04	–8.164E-06
5	–2.724E-04	–1.671E-04	–1.602E-05
6	–2.262E-04	–1.378E-04	1.156E-05
7	–1.781E-04	–1.075E-04	1.156E-05
8	–3.492E-04	–2.017E-04	–2.254E-05
9	–2.428E-04	–1.100E-04	0.000E-01
10	–2.428E-04	–1.100E-04	0.000E-01
11	–2.468E-04	–1.137E-04	0.000E-01
12	–2.389E-04	–1.064E-04	0.000E-01
13	–2.428E-04	–9.470E-05	0.000E-01
14	–9.297E-05	–8.421E-05	0.000E-01
15	–9.297E-05	–8.421E-05	0.000E-01
16	5.224E-05	–2.467E-05	0.000E-01
17	5.224E-05	–2.467E-05	0.000E-01
18	5.224E-05	–2.467E-05	0.000E-01
19	5.224E-05	–2.467E-05	0.000E-01
20	5.224E-05	–2.467E-05	0.000E-01

Table 10. Mode shape coefficients, mode 1, longitudinal shake, 0-deg yaw, snubbers engaged

Node	X coefficient	Y coefficient	Z coefficient
1	–6.369E-04	8.882E-05	–1.997E-05
2	–6.370E-04	8.882E-05	–1.998E-05
3	–6.370E-04	8.882E-05	–1.998E-05
4	–6.370E-04	8.882E-05	–1.219E-05
5	–6.370E-04	8.882E-05	–2.706E-05
6	–6.064E-04	1.199E-05	–2.074E-05
7	–5.932E-04	3.320E-05	–2.033E-05
8	–5.932E-04	6.509E-05	–4.067E-05
9	–5.766E-04	7.090E-05	0.000E-01
10	–5.766E-04	7.090E-05	0.000E-01
11	–5.766E-04	5.850E-05	0.000E-01
12	–5.765E-04	8.328E-05	0.000E-01
13	–5.766E-04	2.479E-05	0.000E-01
14	–2.883E-04	2.628E-05	0.000E-01
15	–2.883E-04	2.628E-05	0.000E-01
16	–9.040E-06	8.515E-06	0.000E-01
17	–9.040E-06	8.515E-06	0.000E-01
18	–9.040E-06	8.515E-06	0.000E-01
19	–9.040E-06	8.515E-06	0.000E-01
20	–9.040E-06	8.048E-06	0.000E-01

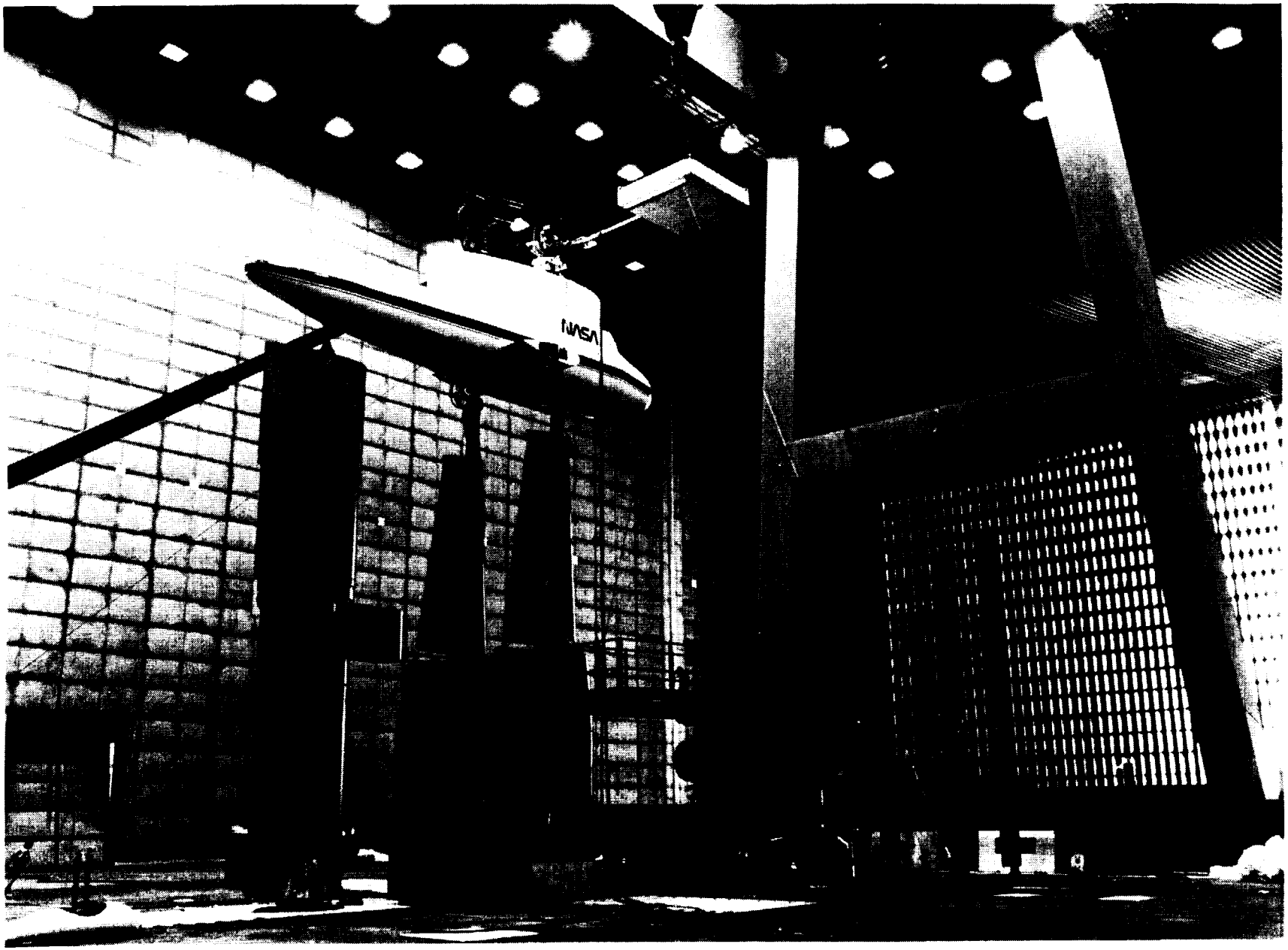

Figure 1. Shake test setup of RTA in the 80- by 120-Foot Wind Tunnel.

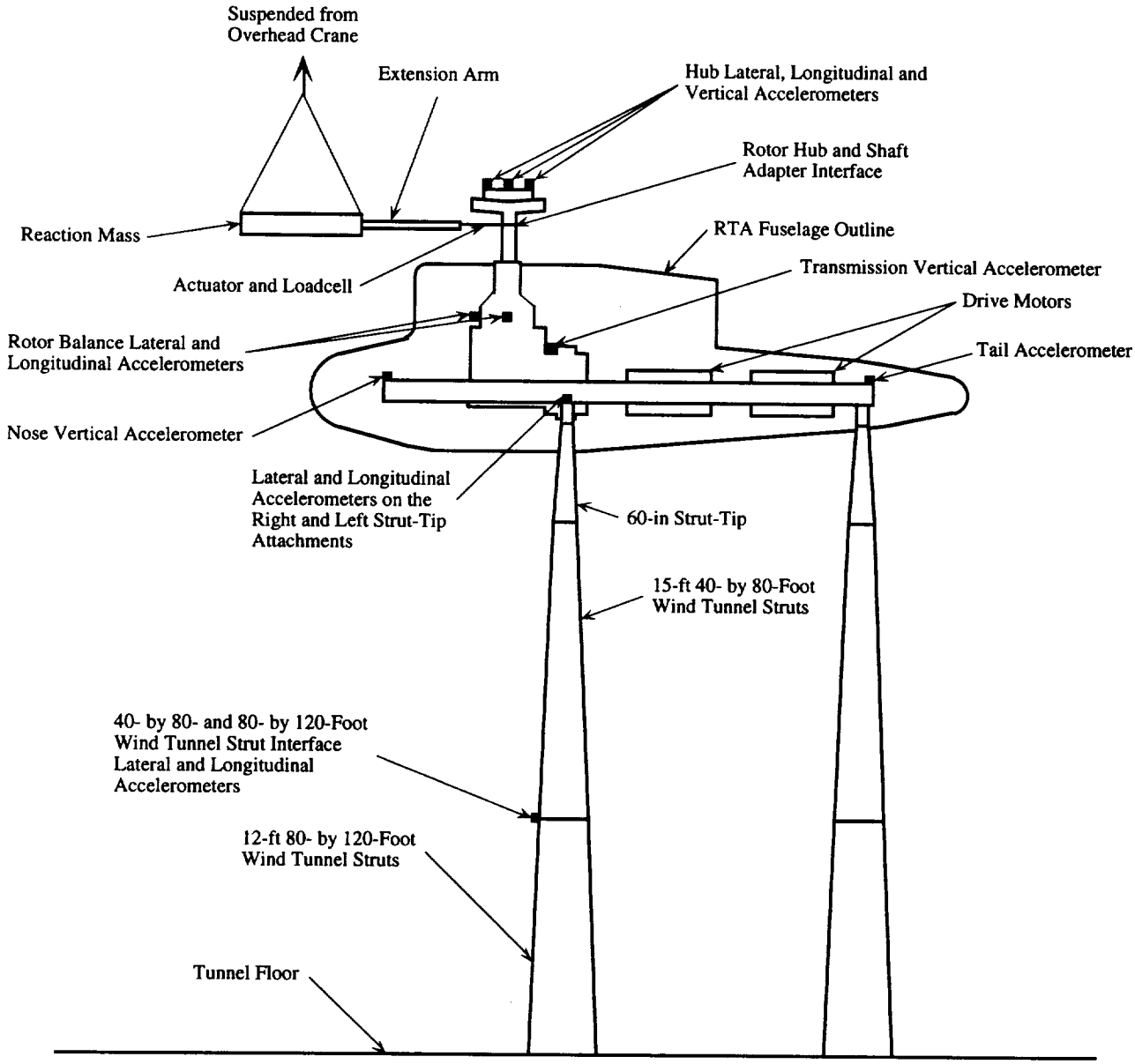

Figure 2. Schematic of RTA shake test setup in the 80- by 120-Foot Wind Tunnel.

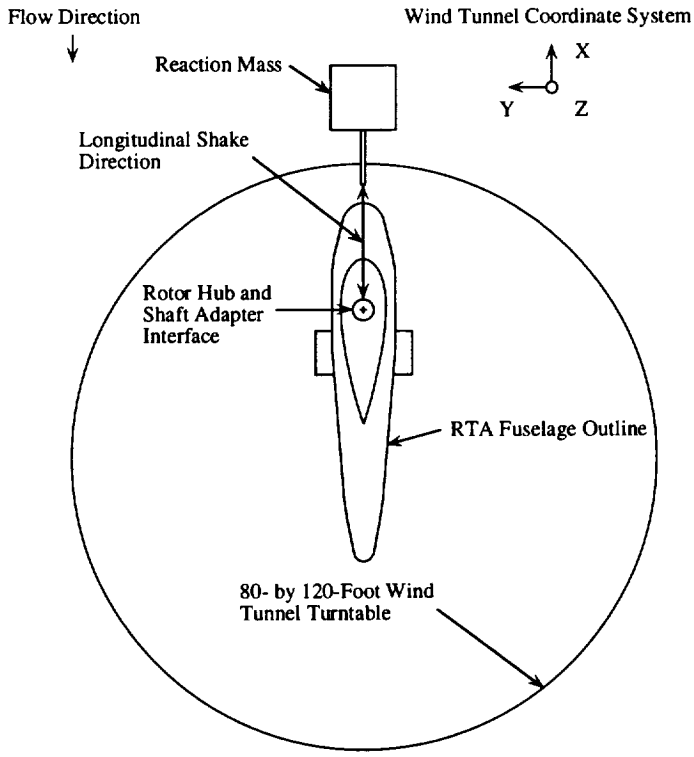

Figure 3(a). Schematic of top view of RTA longitudinal 0-deg yaw shake configuration in the 80- by 120-Foot Wind Tunnel.

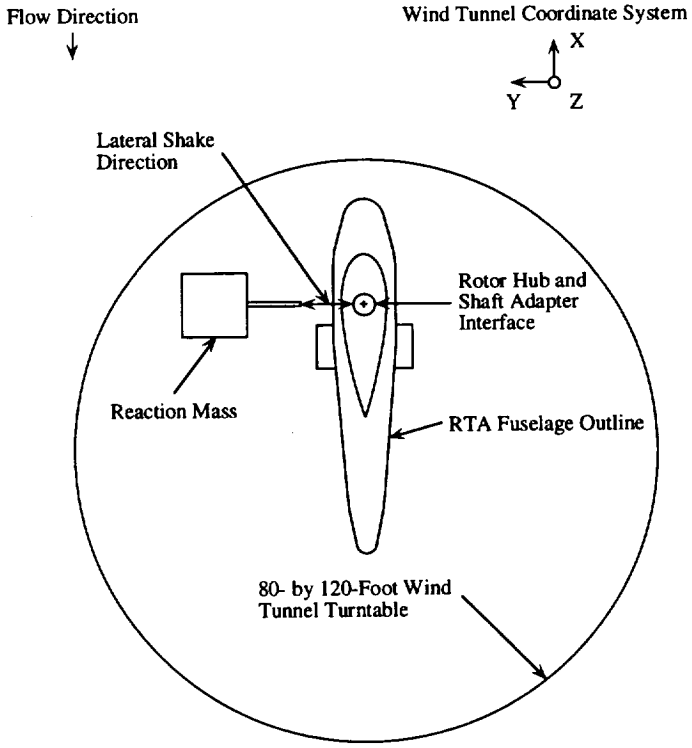

Figure 3(b). Schematic of top view of RTA lateral 0-deg yaw shake configuration in the 80- by 120-Foot Wind Tunnel.

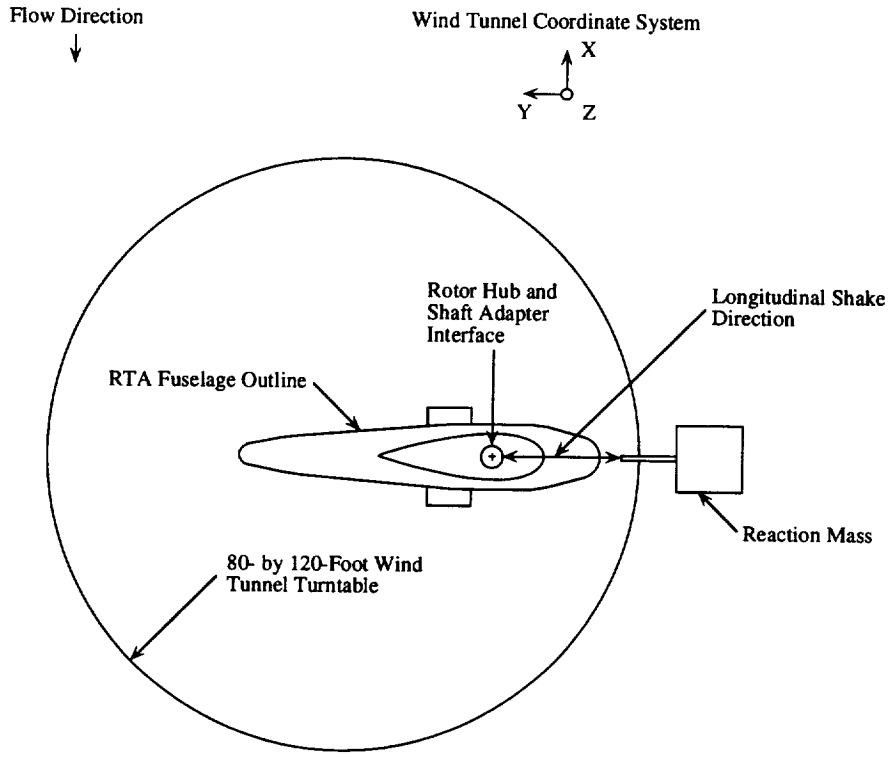

Figure 4(a). Schematic of top view of RTA longitudinal 90-deg yaw shake configuration in the 80- by 120-Foot Wind Tunnel.

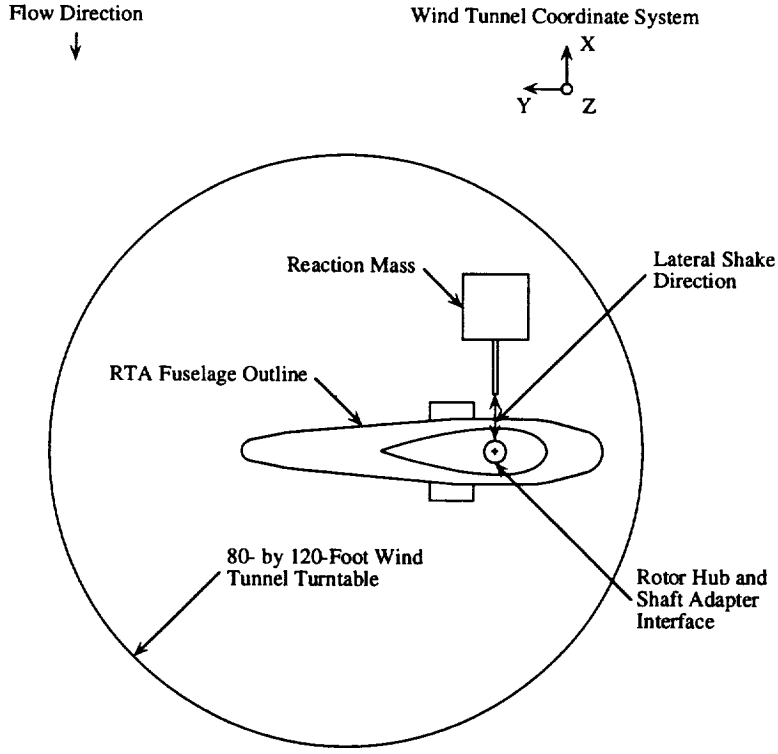

Figure 4(b). Schematic of top view of RTA lateral 90-deg yaw shake configuration in the 80- by 120-Foot Wind Tunnel.

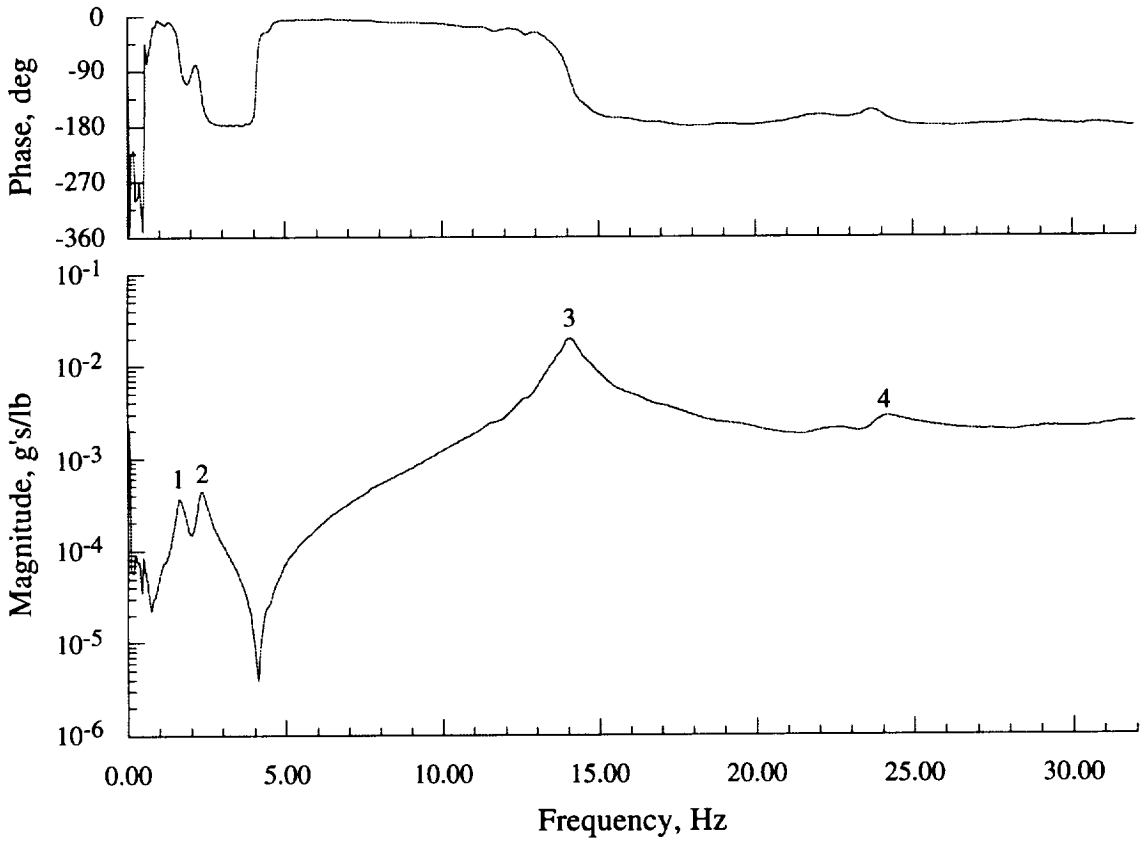

Mode	Frequency, Hz	Magnitude, g/lb	Phase, deg
1	1.6250	0.0003636	–46.17
2	2.3125	0.0004429	–111.90
3	14.0625	0.0199330	–95.87
4	24.1875	0.0028700	–165.60

Figure 5. Frequency response function of hub lateral response to lateral excitation, 0-deg yaw shake configuration, snubbers disengaged.

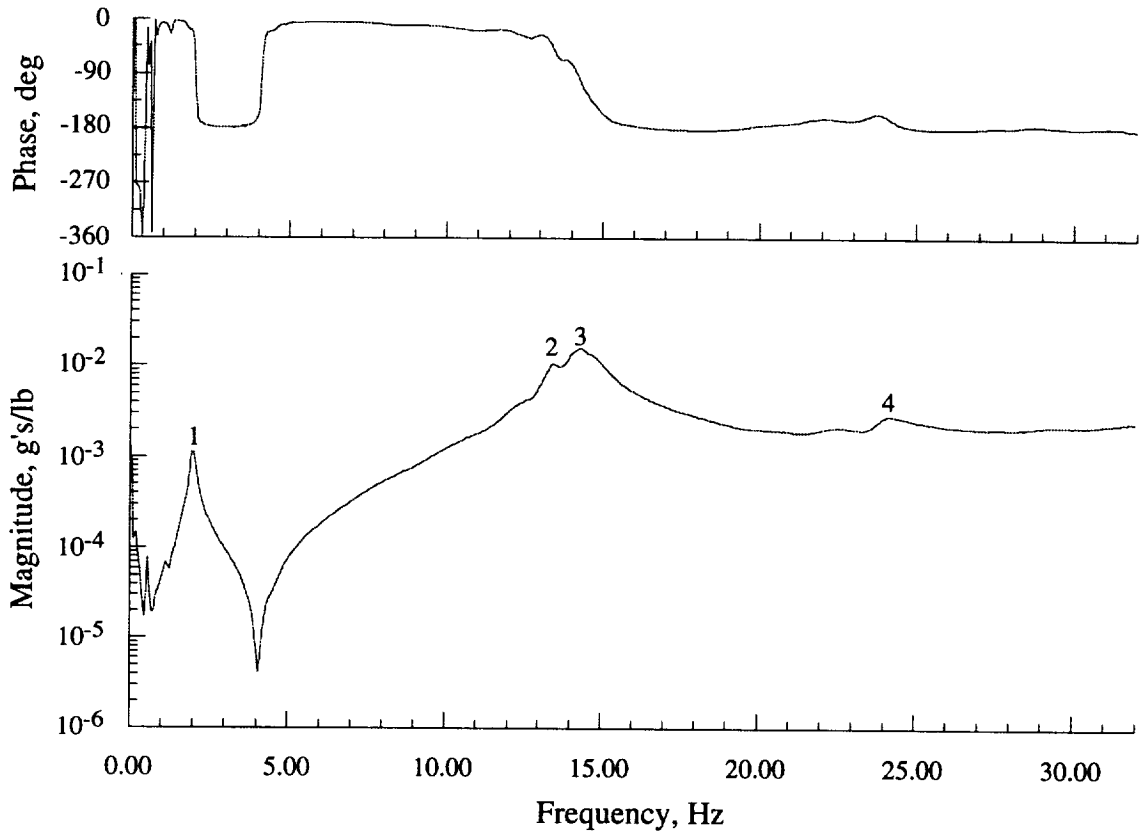

Mode	Frequency, Hz	Magnitude, g/lb	Phase, deg
1	2.0000	0.0011480	–119.70
2	13.4375	0.0105750	–53.54
3	14.3125	0.0156170	–107.00
4	24.1875	0.0028327	–164.80

Figure 6. Frequency response function of hub lateral response to lateral excitation, 0-deg yaw shake configuration, snubbers engaged.

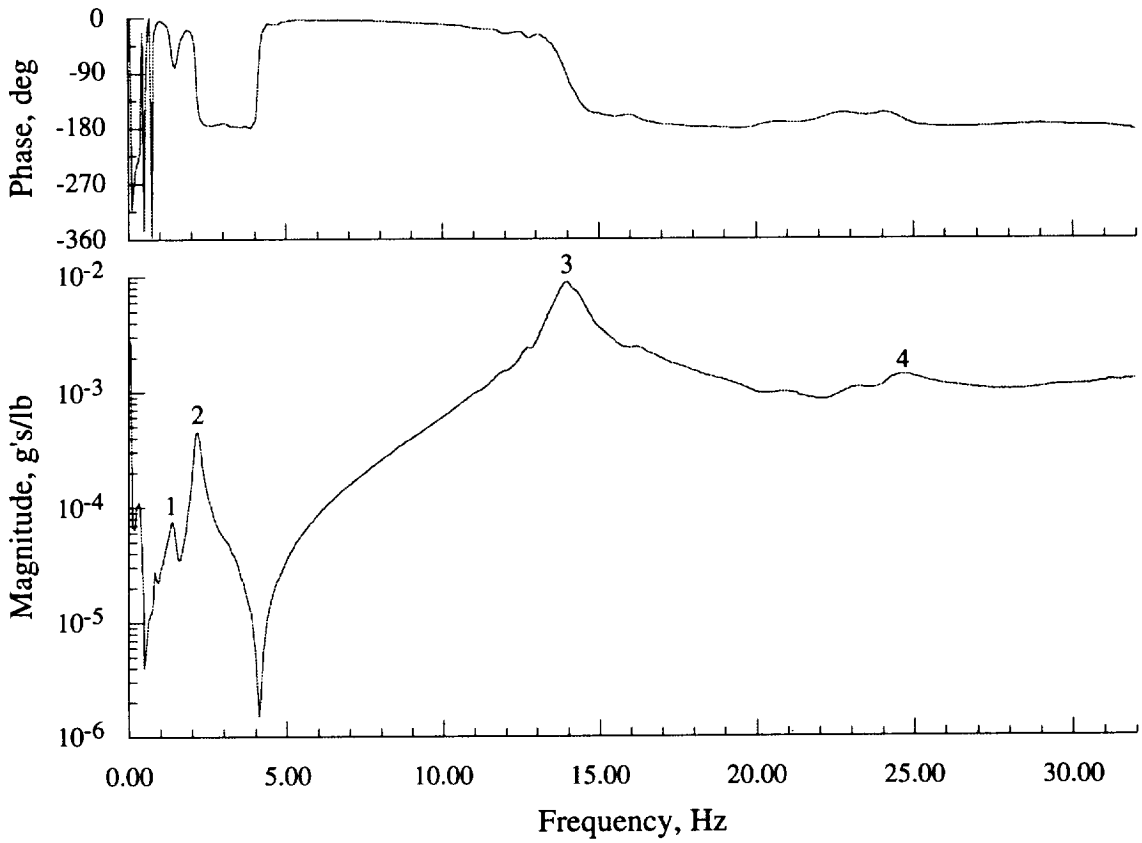

Mode	Frequency, Hz	Magnitude, g/lb	Phase, deg
1	1.3750	0.0000763	–48.04
2	2.1875	0.0004471	–135.10
3	13.9375	0.0088067	–87.53
4	24.7500	0.0013896	–168.80

Figure 7. Frequency response function of hub lateral response to lateral excitation, 90-deg yaw shake configuration, snubbers disengaged.

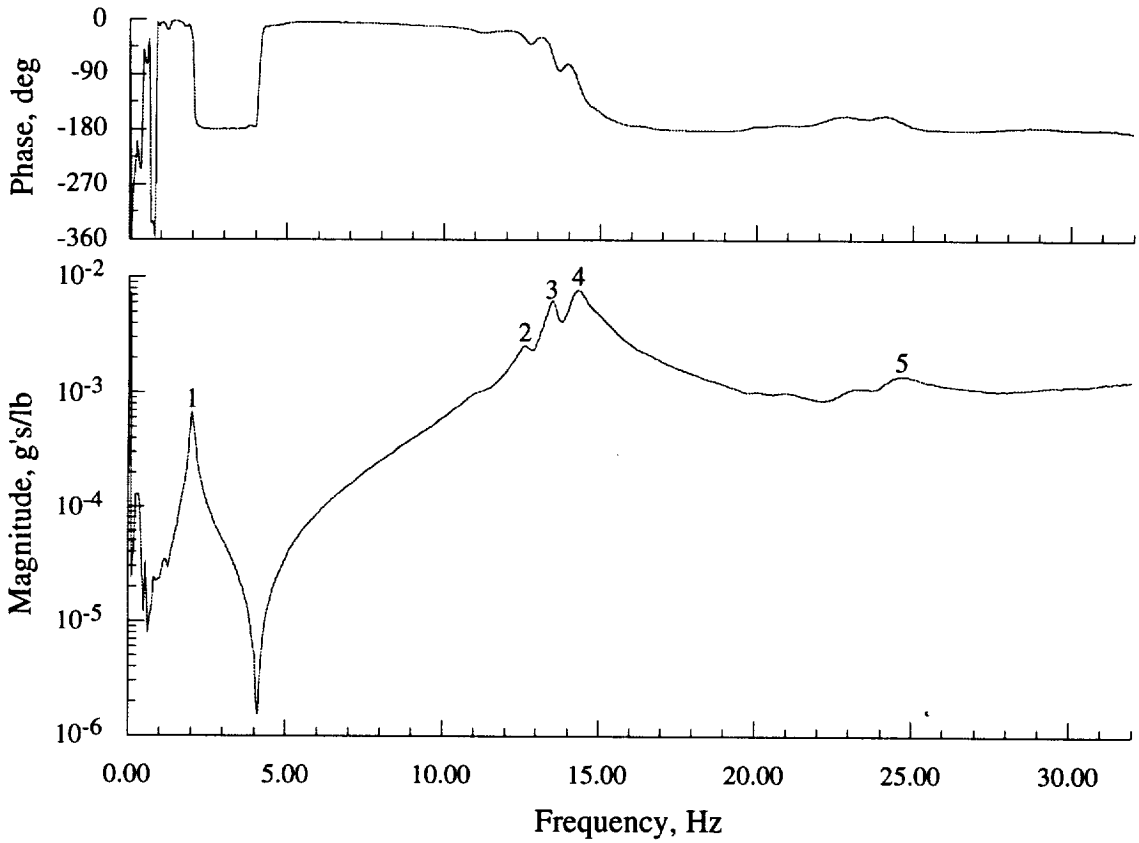

Mode	Frequency, Hz	Magnitude, g/lb	Phase, deg
1	2.0000	0.0006701	–37.40
2	12.6250	0.0025223	–34.19
3	13.5000	0.0062642	–64.50
4	14.3125	0.0077680	–105.70
5	24.6250	0.0013942	–165.50

Figure 8. Frequency response function of hub lateral response to lateral excitation, 90-deg yaw shake configuration, snubbers engaged.

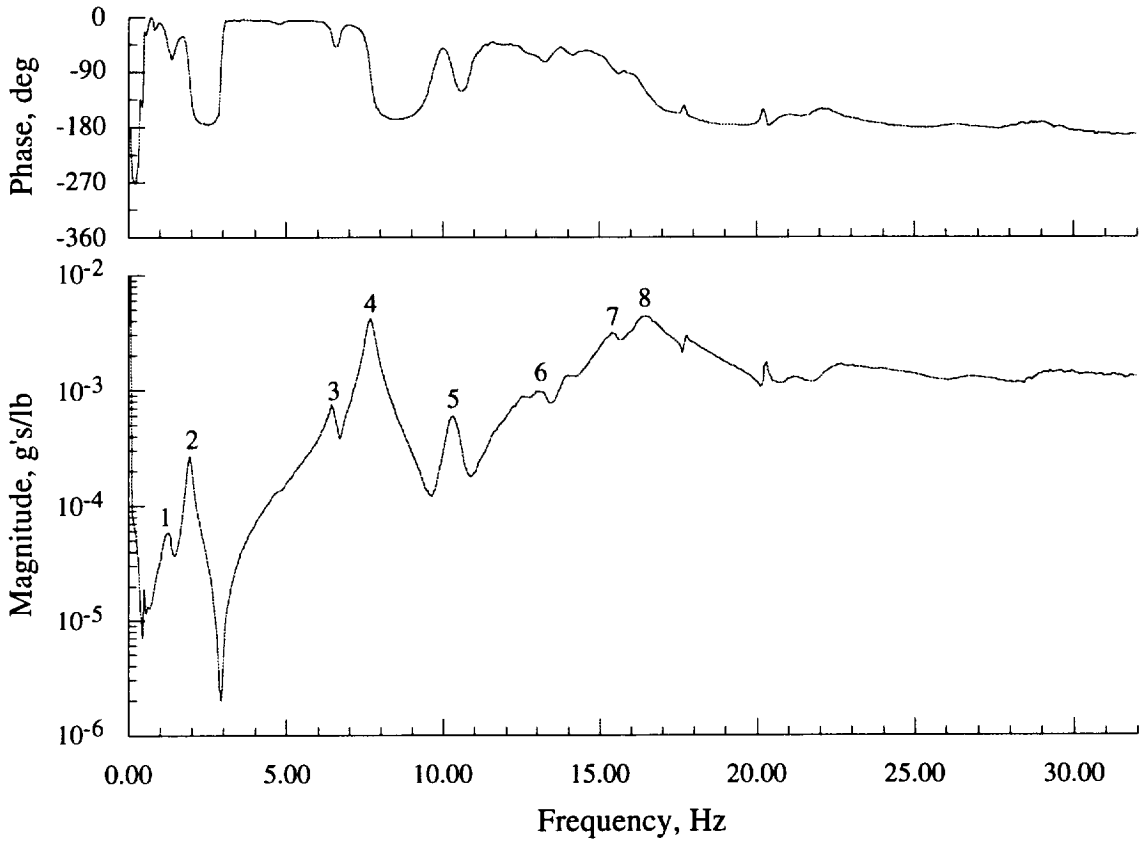

Mode	Frequency, Hz	Magnitude, g/lb	Phase, deg
1	1.2500	0.0000590	–50.91
2	1.9375	0.0002712	–100.60
3	6.4375	0.0007428	–26.83
4	7.6875	0.0041491	–95.51
5	10.3125	0.0005927	–90.46
6	13.0000	0.0031171	–82.17
7	15.3750	0.0043854	–119.00
8	16.4375	0.0009666	–64.46

Figure 9. Frequency response function of hub longitudinal response to longitudinal excitation, 0-deg yaw shake configuration, snubbers disengaged.

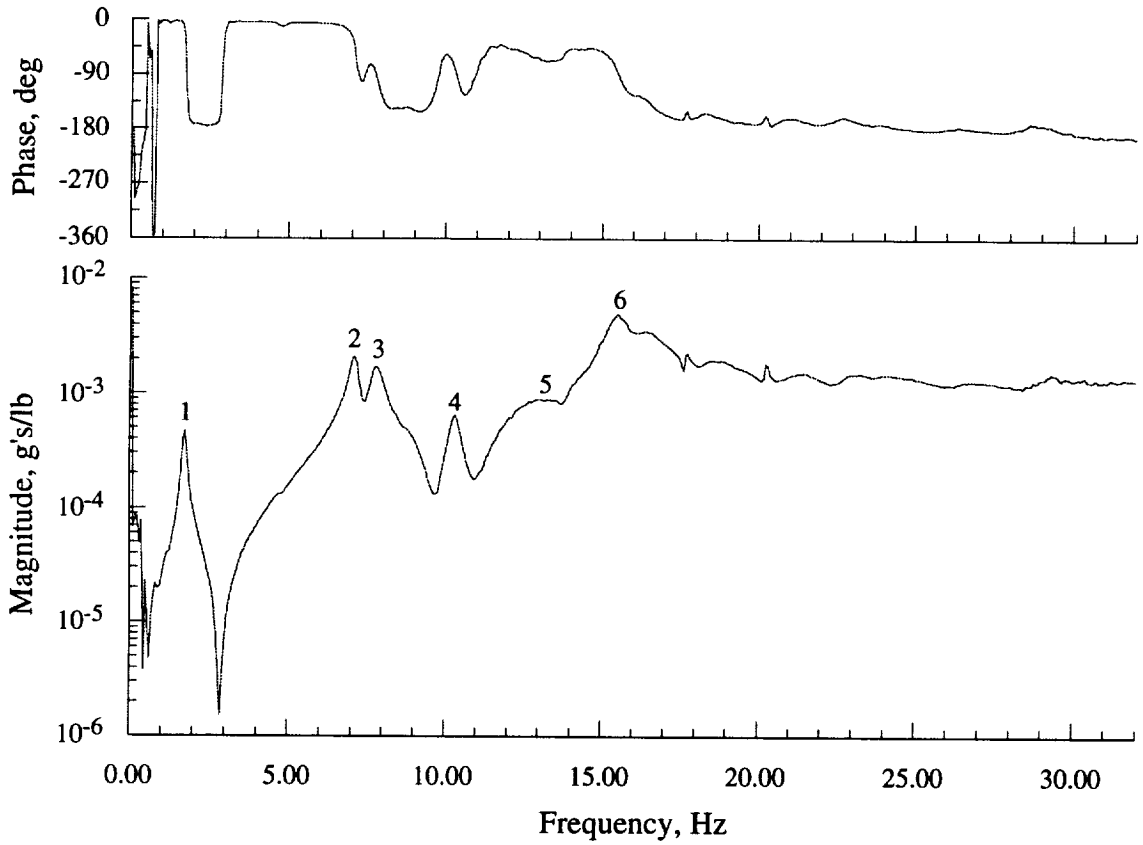

Mode	Frequency, Hz	Magnitude, g/lb	Phase, deg
1	1.7500	0.0004629	–124.50
2	7.1250	0.0020871	–74.56
3	7.8125	0.0017102	–105.90
4	10.3125	0.0006334	–92.63
5	12.9375	0.0008896	–61.72
6	15.5000	0.0049129	–90.01

Figure 10. Frequency response function of hub longitudinal response to longitudinal excitation, 0-deg yaw shake configuration, snubbers engaged.

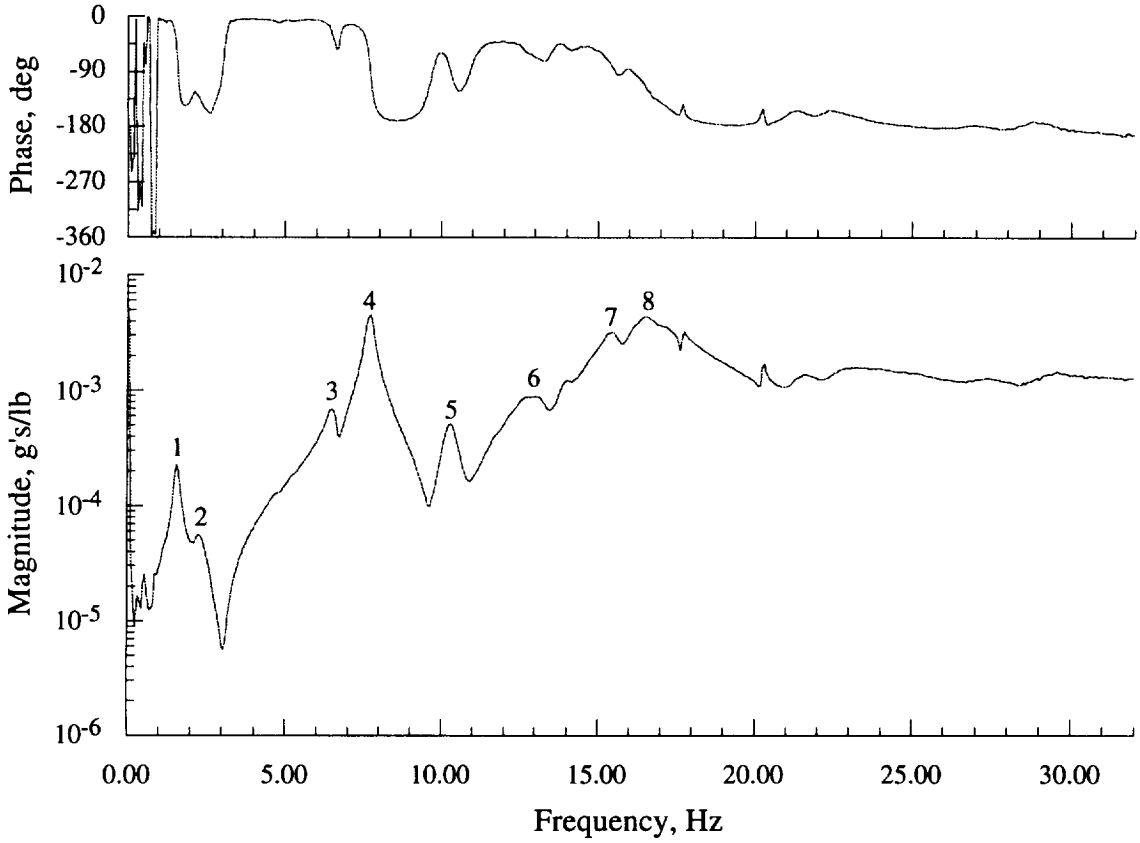

Mode	Frequency, Hz	Magnitude, g/lb	Phase, deg
1	1.5625	0.0002269	–61.23
2	2.2500	0.0000561	–130.90
3	6.5000	0.0006759	–32.28
4	7.7500	0.0045170	–116.50
5	10.3125	0.0005028	–99.00
6	12.9375	0.0008776	–63.70
7	15.5000	0.0031802	–86.44
8	16.5625	0.0043904	–119.40

Figure 11. Frequency response function of hub longitudinal response to longitudinal excitation, 90-deg yaw shake configuration, snubbers disengaged.

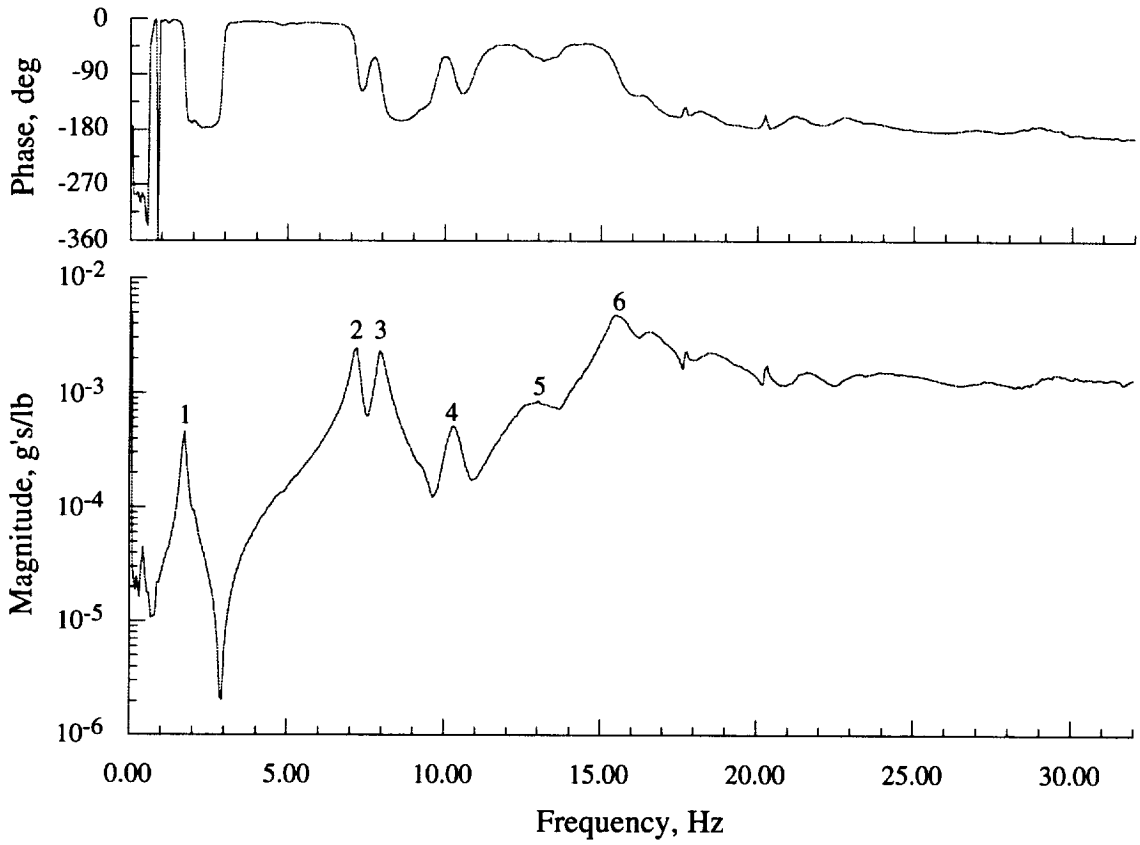

Mode	Frequency, Hz	Magnitude, g/lb	Phase, deg
1	1.7500	0.0004568	–126.10
2	7.1875	0.0024323	–84.94
3	7.9375	0.0023323	–101.20
4	10.3125	0.0005084	–98.47
5	13.0000	0.0008258	–62.93
6	15.5000	0.0047537	–86.18

Figure 12. Frequency response function of hub longitudinal response to longitudinal excitation, 90-deg yaw shake configuration, snubbers engaged.

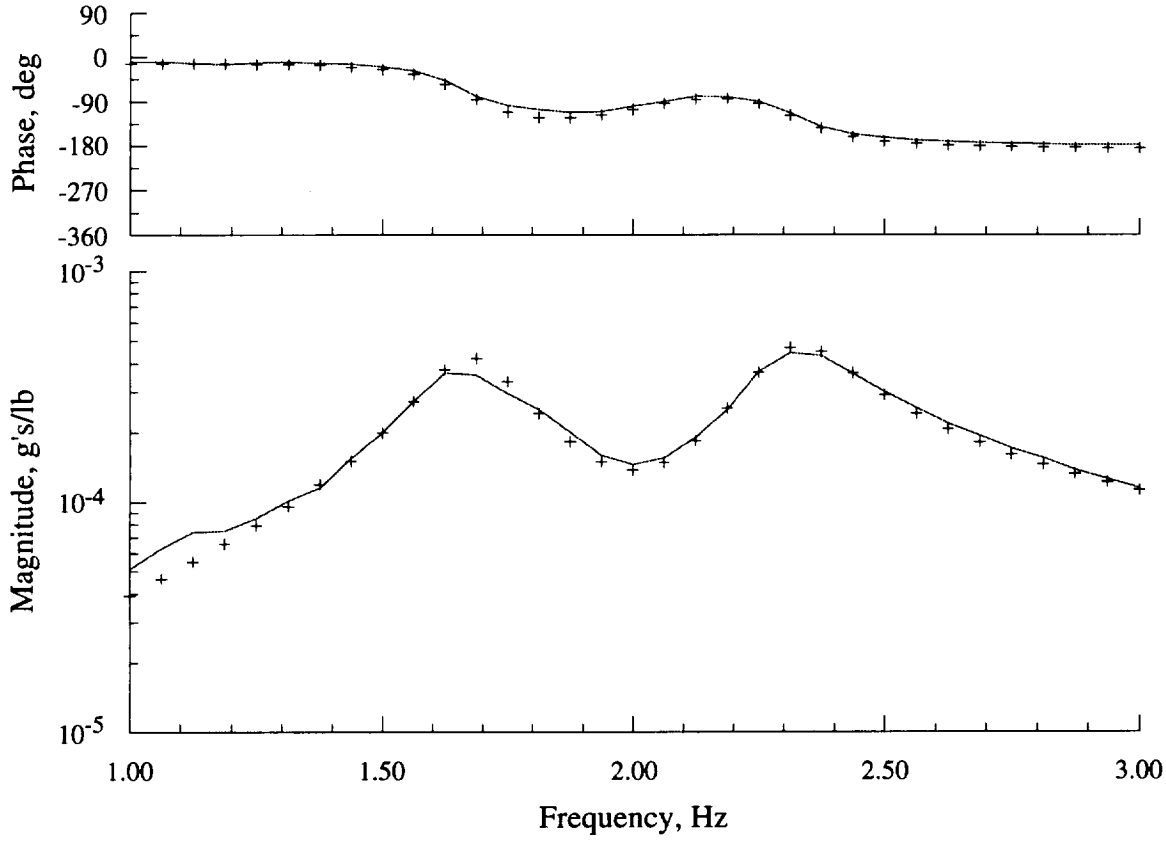

Figure 13. Curve-fit ("+" signs) of hub lateral frequency response function, 0-deg yaw shake configuration, snubbers disengaged (frequency range: 1.0–3.0 Hz).

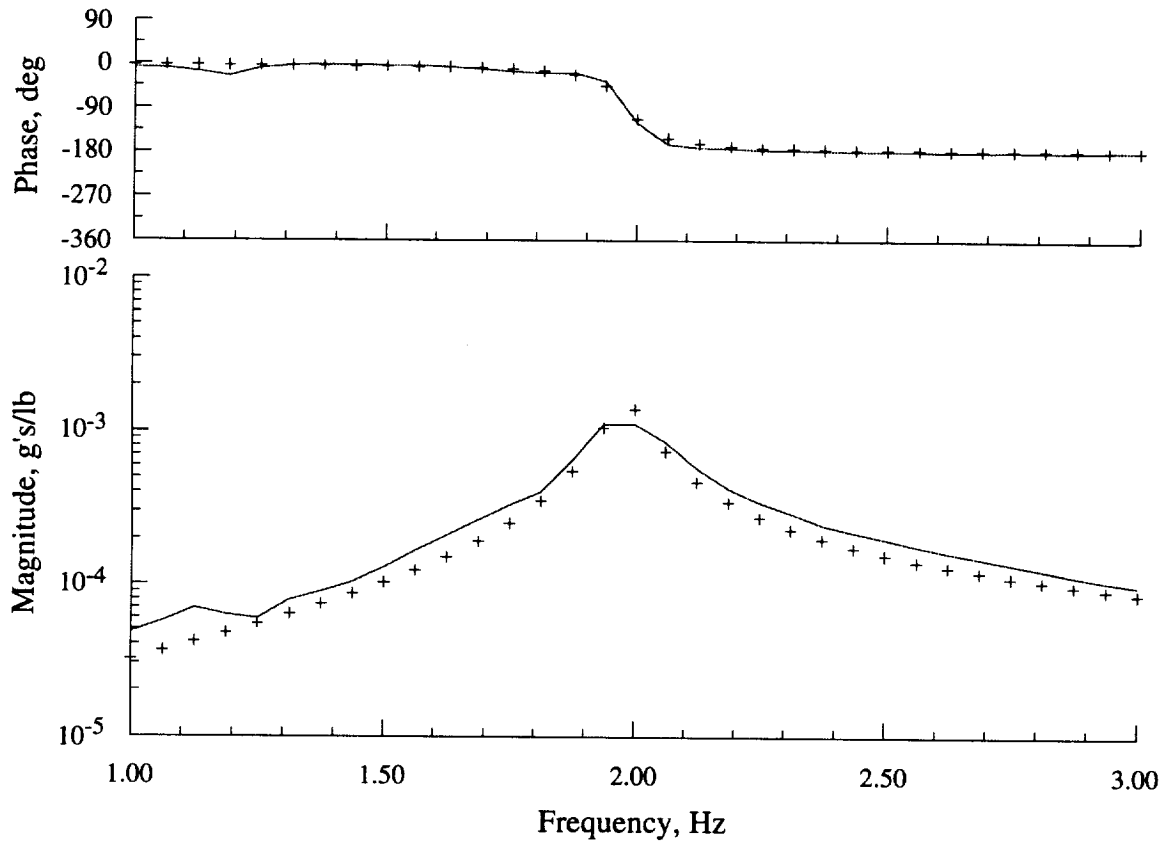

Figure 14. Curve-fit ("+" signs) of hub lateral frequency response function, 0-deg yaw shake configuration, snubbers engaged (frequency range: 1.0–3.0 Hz).

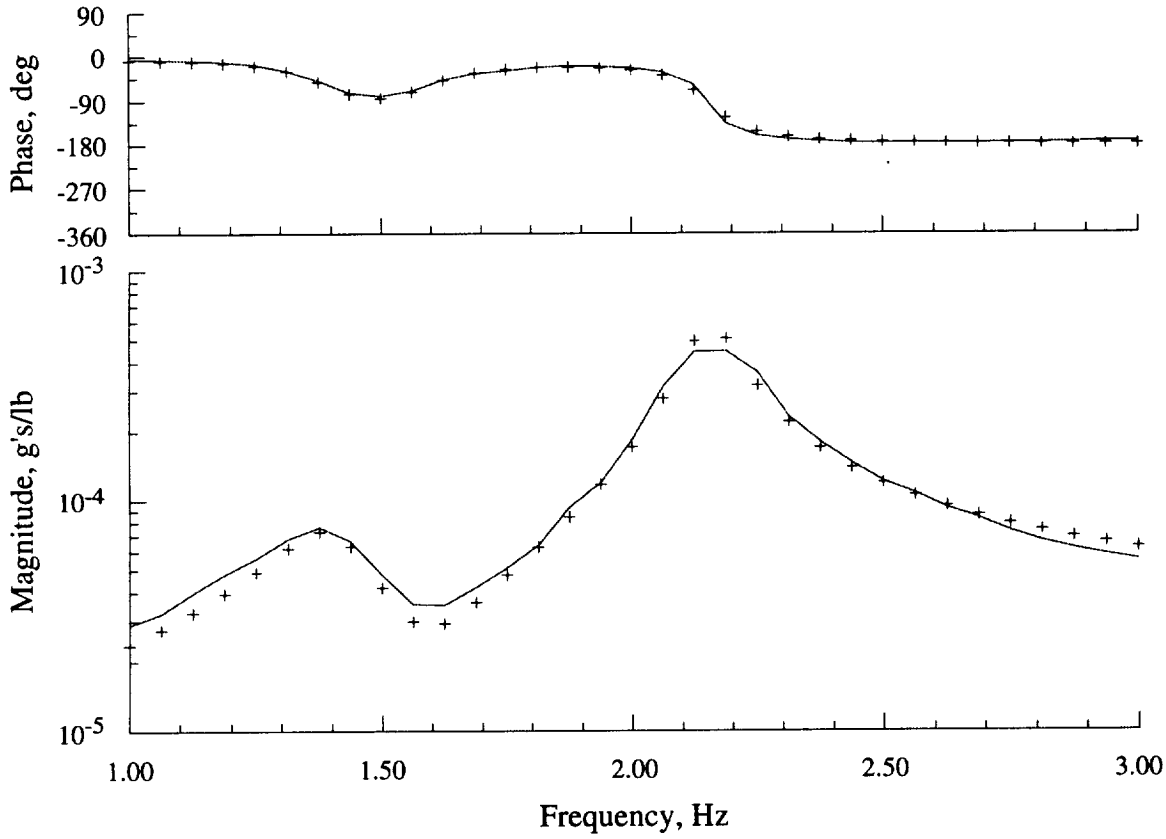

Figure 15. Curve-fit ("+" signs) of hub lateral frequency response function, 90-deg yaw shake configuration, snubbers disengaged (frequency range: 1.0–3.0 Hz).

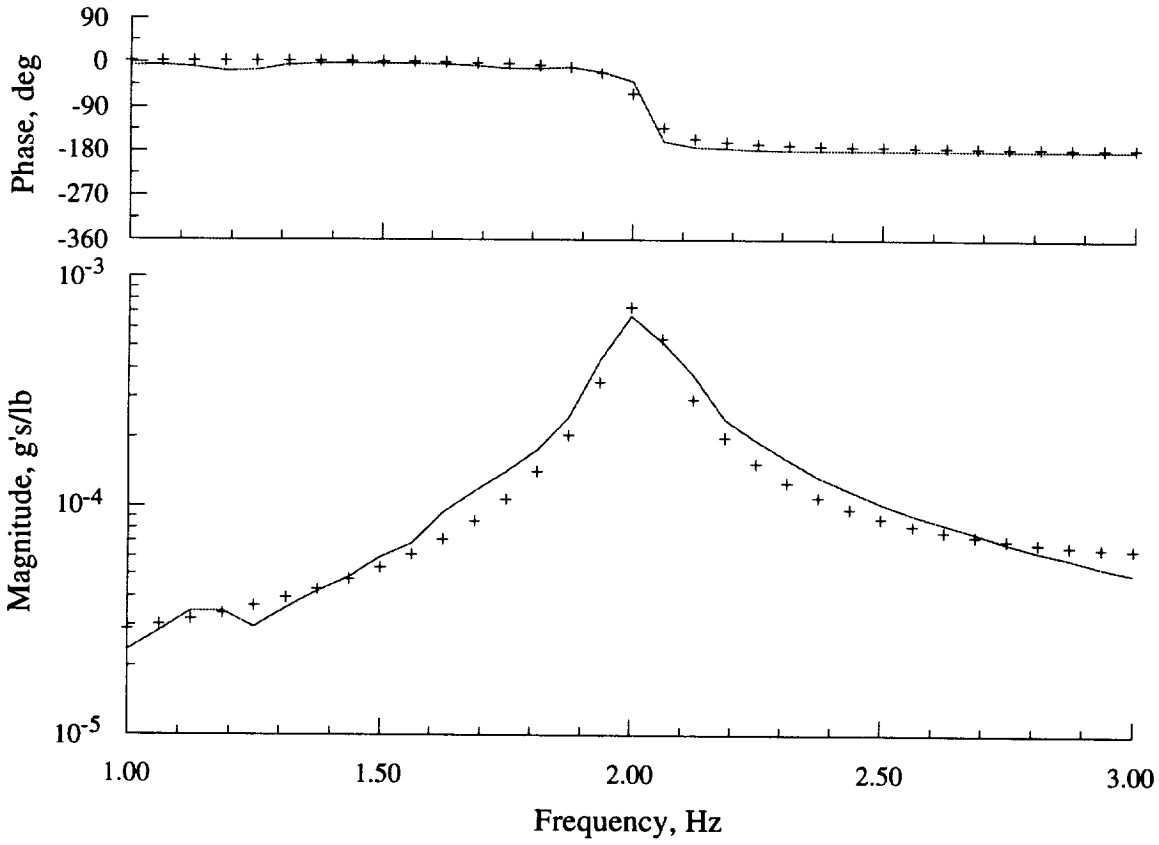

Figure 16. Curve-fit ("+" signs) of hub lateral frequency response function, 90-deg yaw shake configuration, snubbers engaged (frequency range: 1.0–3.0 Hz).

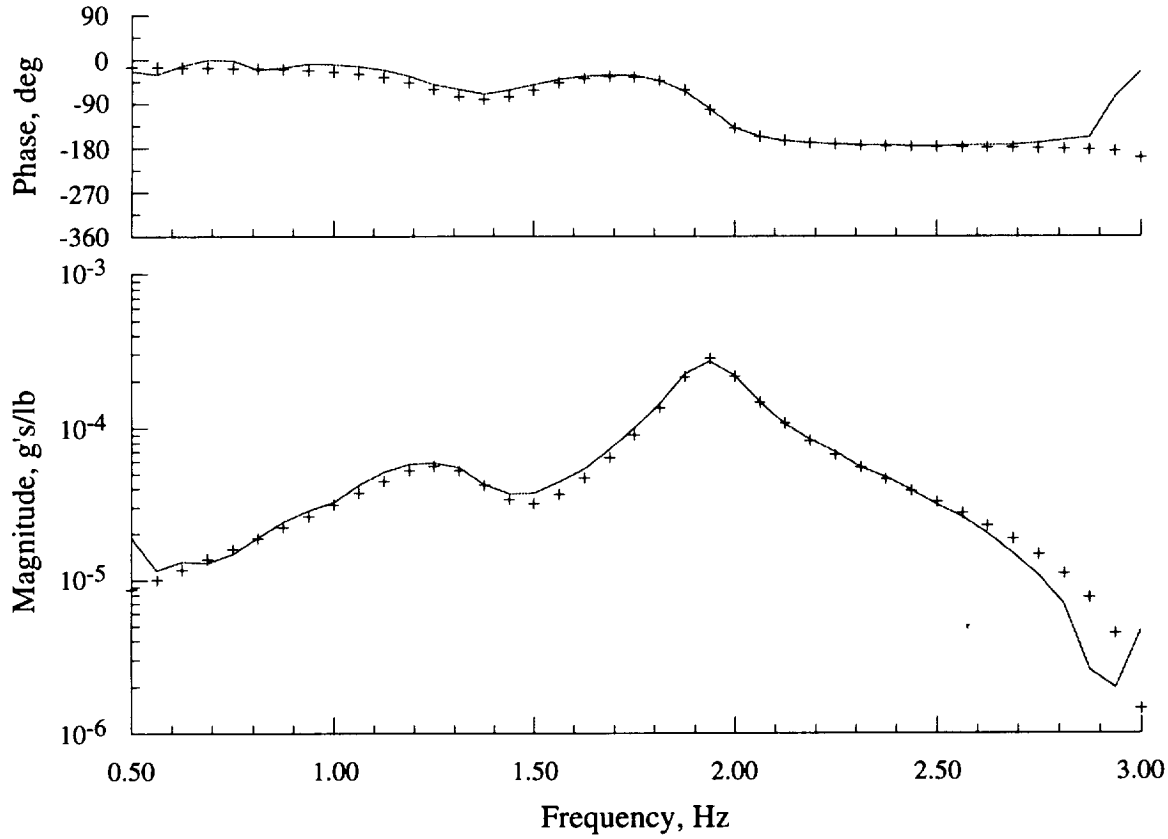

Figure 17. Curve-fit ("+" signs) of hub longitudinal frequency response function, 0-deg yaw shake configuration, snubbers disengaged (frequency range: 0.5–3.0 Hz).

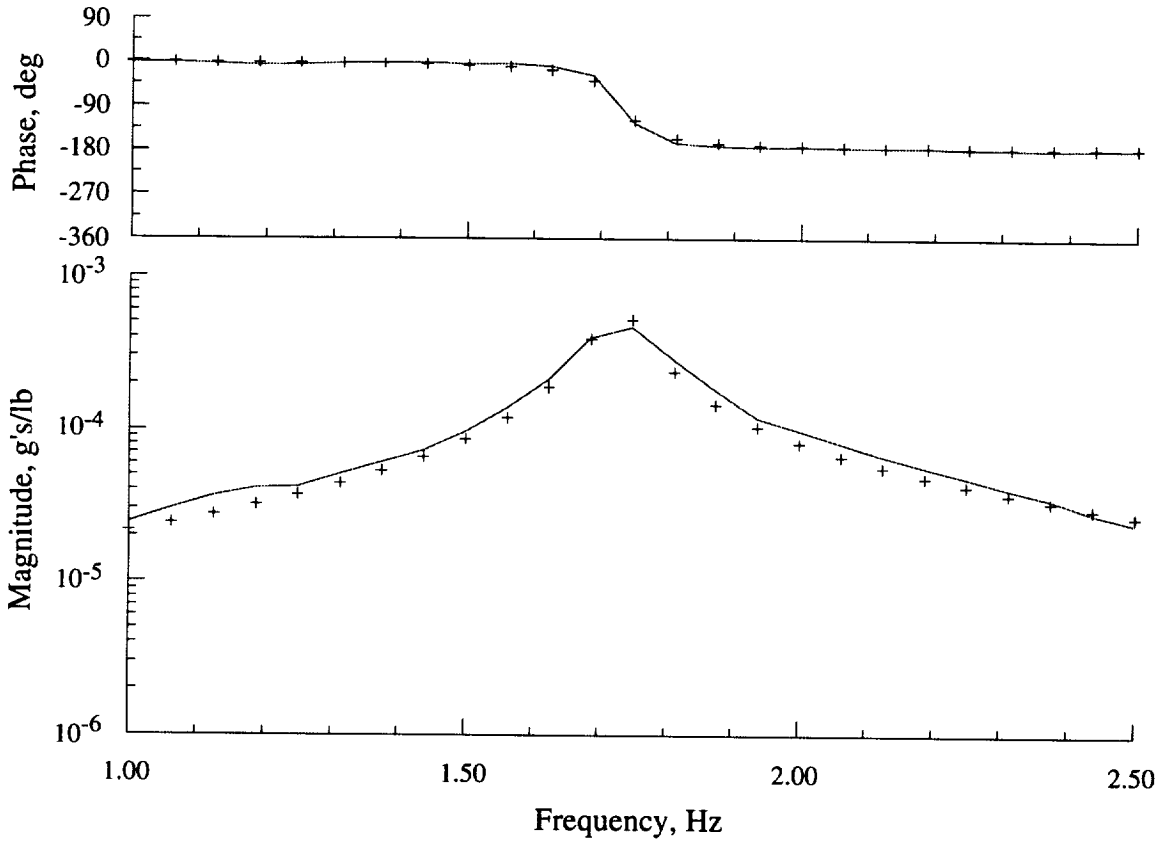

Figure 18. Curve-fit ("+" signs) of hub longitudinal frequency response function, 0-deg yaw shake configuration, snubbers engaged (frequency range: 1.0–2.5 Hz).

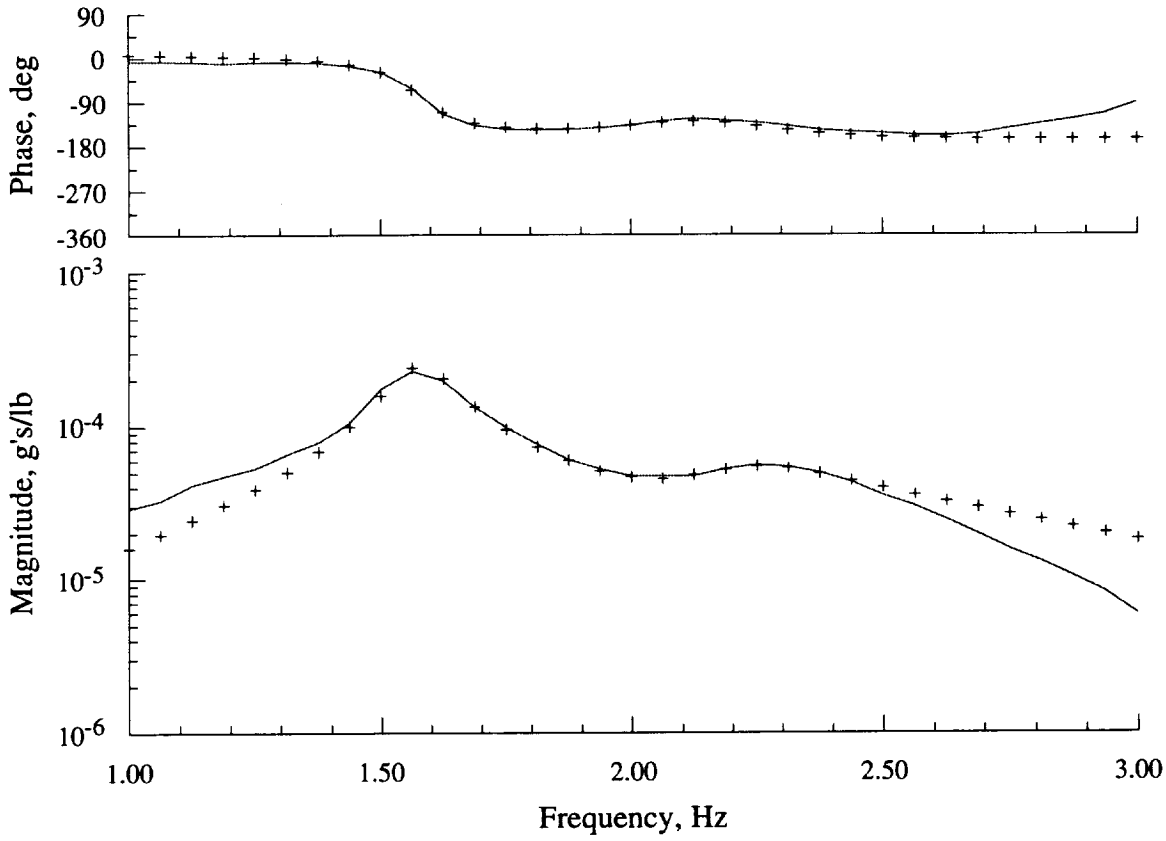

Figure 19. Curve-fit ("+" signs) of hub longitudinal frequency response function, 90-deg yaw shake configuration, snubbers disengaged (frequency range: 1.0–3.0 Hz).

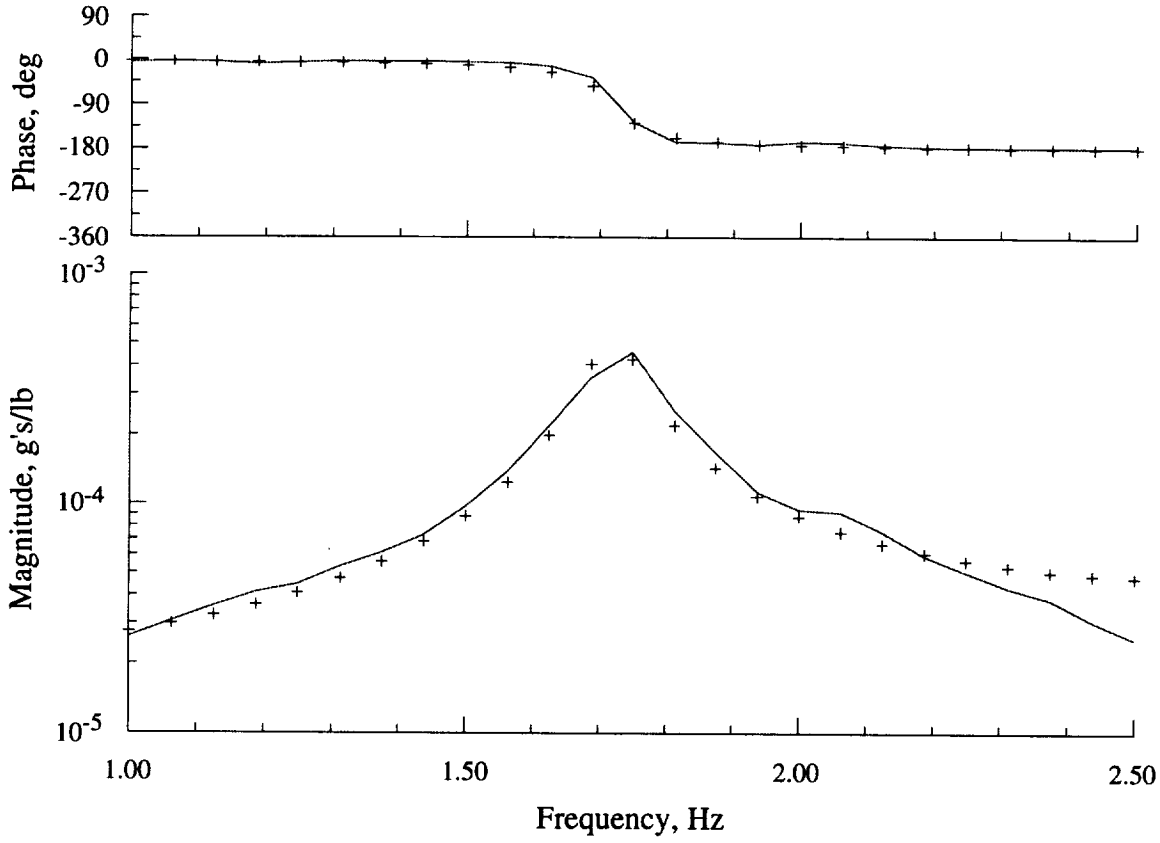

Figure 20. Curve-fit ("+" signs) of hub longitudinal frequency response function, 90-deg yaw shake configuration, snubbers engaged (frequency range: 1.0–2.5 Hz).

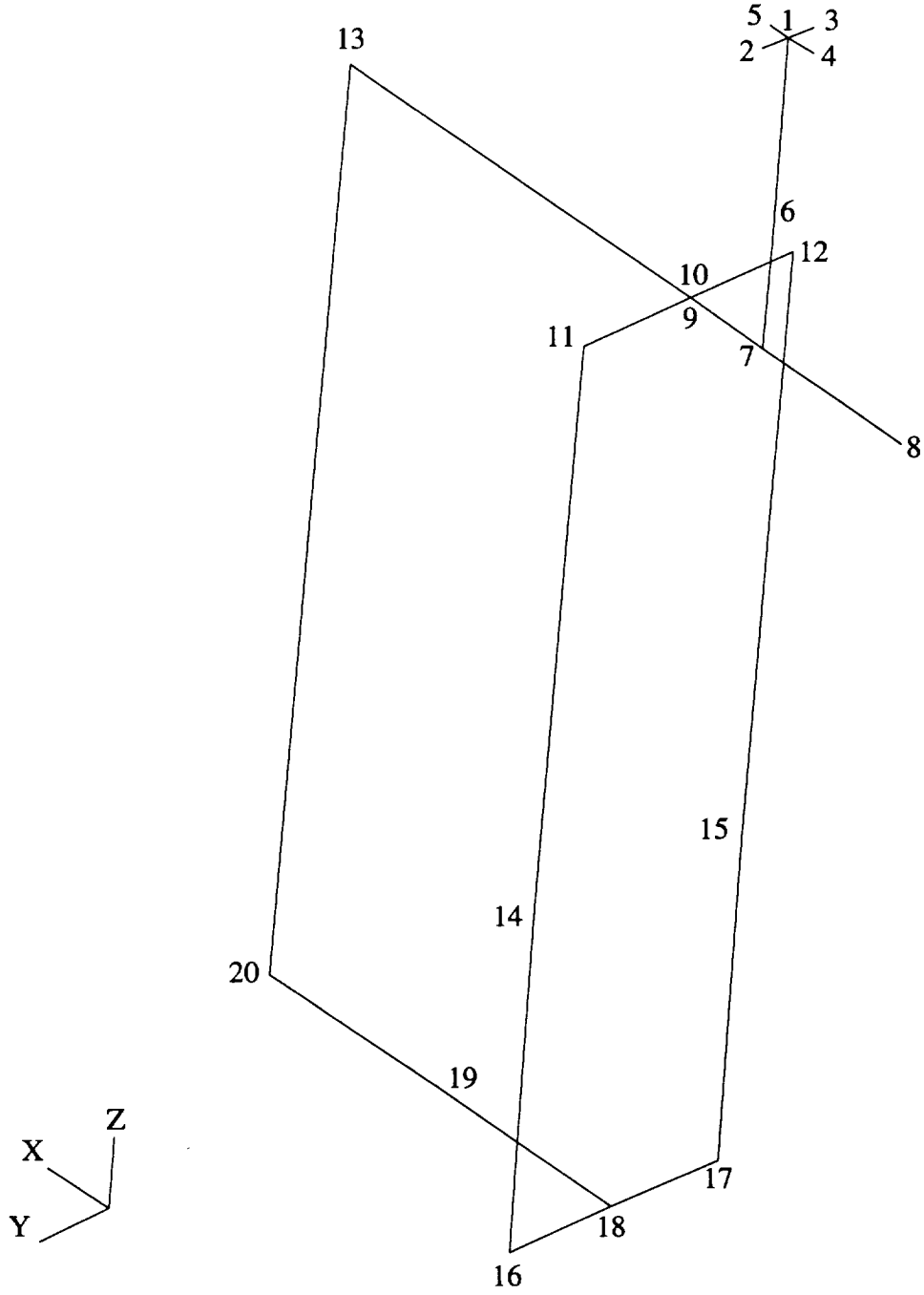

Figure 21. Stick model representation of the RTA in the 80- by 120-Foot Wind Tunnel.

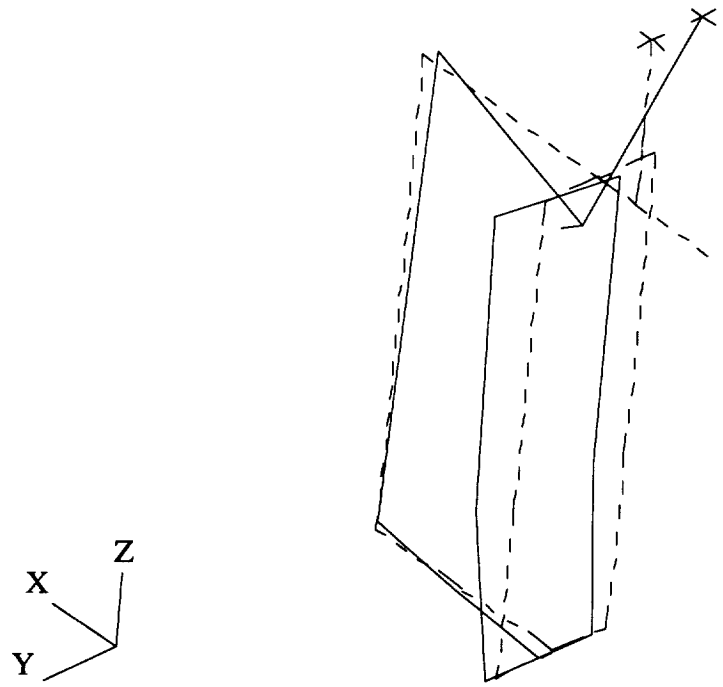

Figure 22. Mode shape display of lateral mode at 1.678 Hz, 0-deg yaw, snubbers disengaged.

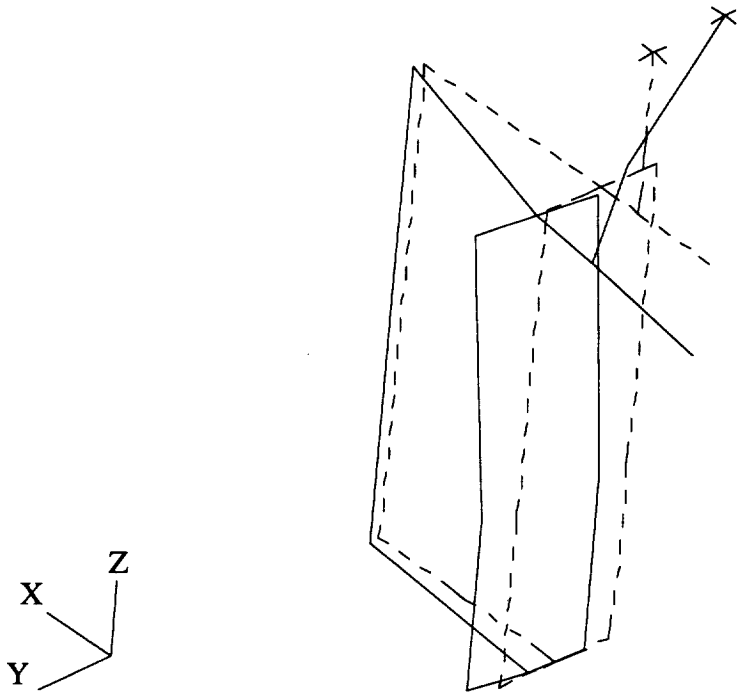

Figure 23. Mode shape display of lateral mode at 2.322 Hz, 0-deg yaw, snubbers disengaged.

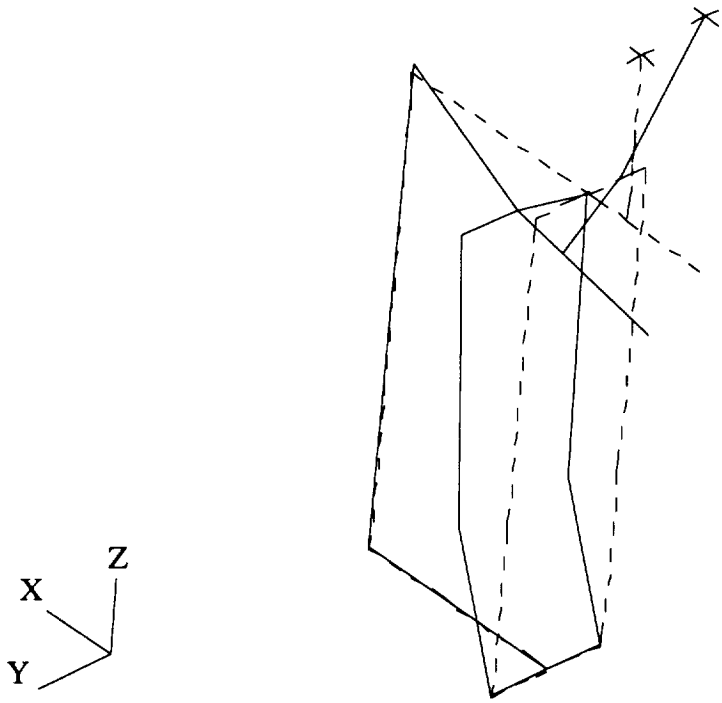

Figure 24. Mode shape display of lateral mode at 1.981 Hz, 0-deg yaw, snubbers engaged.

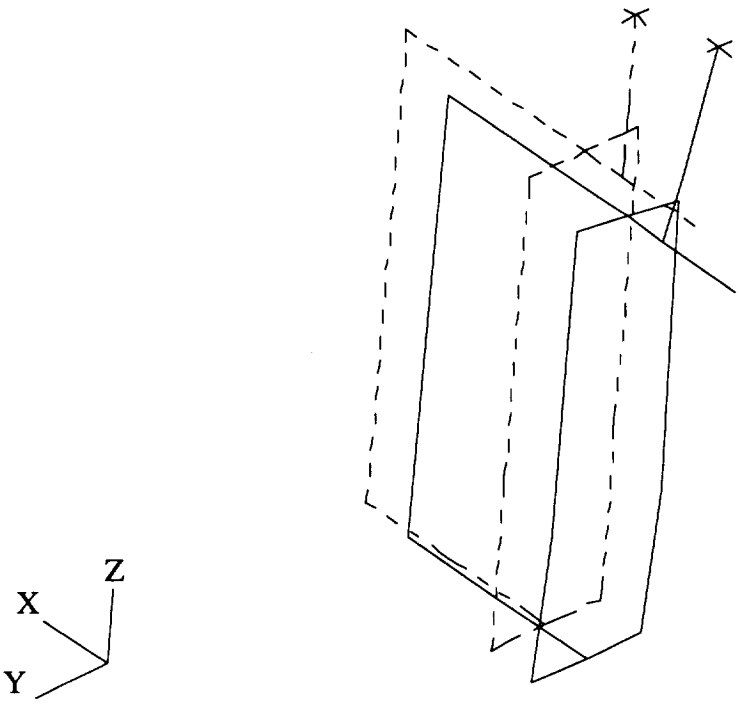

Figure 25. Mode shape display of longitudinal mode at 1.289 Hz, 0-deg yaw, snubbers disengaged.

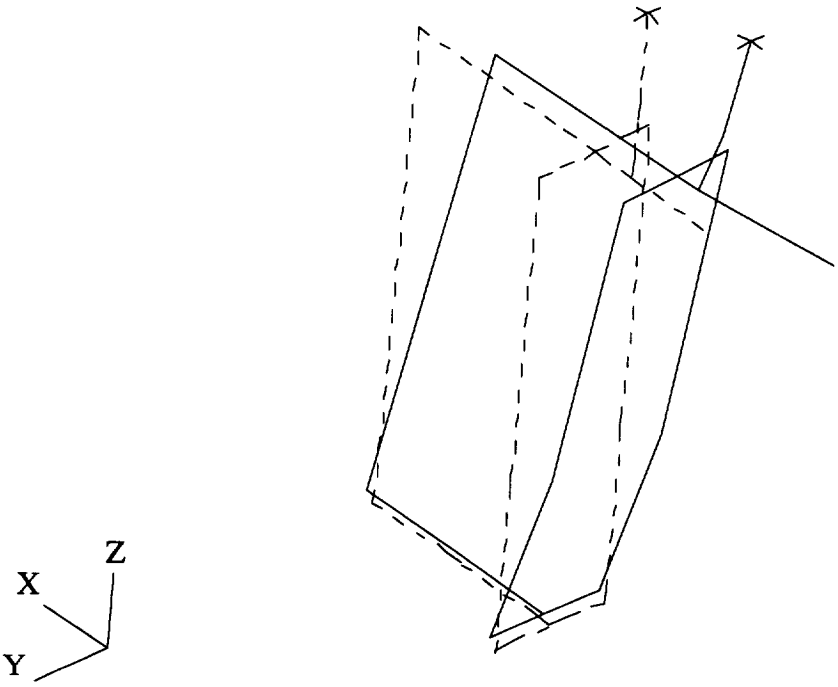

Figure 26. Mode shape display of longitudinal mode at 1.934 Hz, 0-deg yaw, snubbers disengaged.

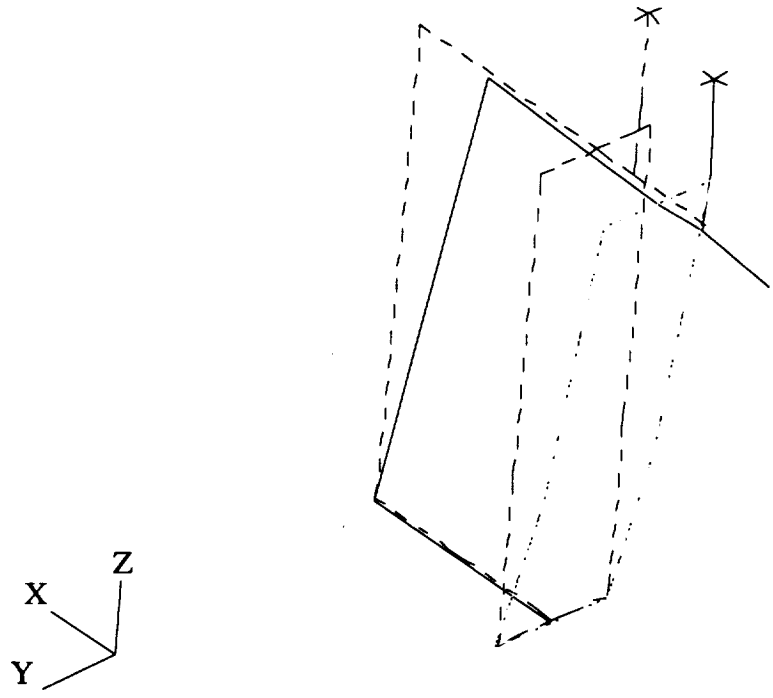

Figure 27. Mode shape display of longitudinal mode at 1.729 Hz, 0-deg yaw, snubbers engaged.

REPORT DOCUMENTATION PAGE

Form Approved
OMB No. 0704-0188

1. AGENCY USE ONLY *(Leave blank)*	2. REPORT DATE	3. REPORT TYPE AND DATES COVERED
	September 1994	Technical Memorandum

4. TITLE AND SUBTITLE

Dynamic Response of NASA Rotor Test Apparatus and Sikorsky S-76 Hub Mounted in the 80- by 120-Foot Wind Tunnel

5. FUNDING NUMBERS

505-59-36

6. AUTHOR(S)

Randall L. Peterson and Muhammed S. Hoque*

7. PERFORMING ORGANIZATION NAME(S) AND ADDRESS(ES)

Ames Research Center
Moffett Field, CA 94035-1000

8. PERFORMING ORGANIZATION REPORT NUMBER

A-94133

9. SPONSORING/MONITORING AGENCY NAME(S) AND ADDRESS(ES)

National Aeronautics and Space Administration
Washington, DC 20546-0001

10. SPONSORING/MONITORING AGENCY REPORT NUMBER

NASA TM-108847

11. SUPPLEMENTARY NOTES

Point of Contact: Randall L. Peterson, Ames Research Center, MS T-12B, Moffett Field, CA 94035-1000; (415) 604-5044
*Sterling Federal Systems, Inc., Palo Alto, California

12a. DISTRIBUTION/AVAILABILITY STATEMENT

Unclassified — Unlimited
Subject Category 39

12b. DISTRIBUTION CODE

13. ABSTRACT ***(Maximum 200 words)***

A shake test was conducted in the 80- by 120-Foot Wind Tunnel at NASA Ames Research Center, using the NASA Ames Rotor Test Apparatus (RTA) and the Sikorsky S-76 rotor hub. The primary objective of this shake test was to determine the modal properties of the RTA, the S-76 rotor hub, and the model support system installed in the wind tunnel. Random excitation was applied at the rotor hub, and vibration responses were measured using accelerometers mounted at various critical locations on the model and the model support system. Transfer functions were computed using the load cell data and the accelerometer responses. The transfer function data were used to compute the system modal parameters with the aid of modal analysis software.

14. SUBJECT TERMS

Modal analysis, Structural response, Dynamics

15. NUMBER OF PAGES

38

16. PRICE CODE

A03

17. SECURITY CLASSIFICATION OF REPORT	18. SECURITY CLASSIFICATION OF THIS PAGE	19. SECURITY CLASSIFICATION OF ABSTRACT	20. LIMITATION OF ABSTRACT
Unclassified	Unclassified		